Title
Spatial and Mechanical Regulation of EphB Receptor in Neural Stem Cell Function

Author
Dong, Meimei

Publication Date
2015

Peer reviewed|Thesis/dissertation

Spatial and Mechanical Regulation of EphB Receptor in Neural Stem Cell Function

By

Meimei Dong

A dissertation submitted in partial satisfaction of the

requirements for the degree of

Doctor of Philosophy

in

Biophysics

in the

Graduate Division

of the

University of California, Berkeley

Committee in charge:

Professor Jay T. Groves, Chair

Professor Sanjay Kumar

Professor David V. Schaffer

Professor Song Li

Spring 2015

Spatial and Mechanical Regulation of EphB Receptor in Neural Stem Cell Function

By

Meimei Dong

Abstract

Spatial and Mechanical Regulation of EphB Receptor in Neural Stem Cell Function

by

Meimei Dong

Doctor of Philosophy in Biophysics

University of California, Berkeley

Professor Jay T. Groves, Chair

EphB4 receptor tyrosine kinases bind and cluster with membrane bound ephrinB2 ligands on apposing cells to signal juxtacrine. While this signal activation plays a regulatory role in neural stem cell differentiation, the underlying biophysical mechanism remains poorly understood. We reconstituted this juxtacrine signalling geometry between live EphB4-expressing neural stem cells and a supported lipid bilayer presenting laterally mobile monomeric ephrinB2 ligands. A novel method was developed to study neural stem cell differentiation by this hybrid system. This setup allows for observations of the timescale and spatial distribution of receptor-ligand binding and clustering. Furthermore, it accommodates the method of spatial mutation—whereby physical constraints are imposed by lithographically patterned micro-corrals—to restrict EphB4 receptor mobility and precisely control the spatial patterns of receptor-ligand organisation. We found that this physical reorganisation of EphB4-ephrinB2 inhibits neuronal differentiation, suggesting spatial and mechanical sensing of EphB4 signalling in neural stem cells.

I dedicate this to my parents and husband, for their unreserved love, encouragement and support.

Table of Contents

Acknowledgements

I would like to thank Professor Jay Groves for his support and guidance during the course of my dissertation research. I am especially grateful for his optimistic and positive encouragement. I would like to thank Professor David Schaffer for being a great collaborator and serving on my dissertation committee. I also would like to thank Professor Sanjay Kumar for being the chair of my committee during my qualifying exam, and Professor Song Li, Professor Matthew Francis, and Professor Polina Lishko for serving on my qualifying exam and dissertation committee.

I would like to thank many past and current Groves' lab members for teaching and helping me in lab during the past three and half years. Sam Lord was my mentor during my rotation in the lab. He taught me how to make lipid bilayers, as well as pretty much all my microscopy knowledge. Michael Coyle was my office mate and we shared lab bench for two years, and he taught me everything about DNA chemistry. I had great help from Michael designing all the fun DNA modifiers for my dissertation project. Aiwei Tian and Adrienne Greene are the other two Eph team members. I learned imaging skills from Aiwei, and molecular biology tricks from Adrienne. William Huang is a great friend in lab, who helped me study physics during my qualifying exam preparation. Jean is a fun new addition to the lab who helped me with the FCS experiments. Shalini Low-Nam provided me much help using Matlab for data analysis. Wan-chen Lin was the bilayer expert in lab, and she helped with bilayer trouble-shooting when I first joined the lab. Young-Kwang Lee fabricated all the nano-substrates for me, without his hard work, I would not be able to do the most critical experiments for my dissertation. The Groves lab members that I have had the honour to work have helped me keep happy doing research every day. I also would like to thank my neural stem cell collaborator Dawn Spelke - thanks for doing all the fun experiments with me!

I would like to thank my parents and my husband for their support. Especially my husband Cliff, who made me an even stronger person and helped me power through all my difficulties throughout graduate school.

Chapter 1: Introduction

Section 1.1: Eph receptor signalling in neural stem cells

Neural stem cells (NSCs) possess extraordinary potential for regenerative neurological therapies and tissue engineering. They are the unique cell types that can self-renew and differentiate into three types of neural cells: neurons, astrocytes, and oligodendrocytes. Adult neural stem cells undergo neurogenesis in the two distinct regions in the mammalian brain, the subgranular zone (SGZ) of hippocampal dentate gyrus, and the subventricular zone (SVZ) of the lateral ventricles (1, 2). The maintenance and fate commitment of NSCs are highly regulated by their microenvironment, which is known as the stem cell niche (Figure 1.1). There are many different niche regulators that can control NSCs behaviour, including soluble factors, membrane-bound ligands and receptors, and extracellular matrix components (3). NSCs show extreme sensitivity to the biophysical and biomechanical cues within their niche, and their functions can be modulated. For example, elastic stiffness regulates neural stem cell fate commitment through extracellular matrix component associated integrin receptor force sensing (4-6). Juxtacrine signalling mediated cell-cell communication is another key niche component: both Notch/jagged and Eph/ephrin signalling have been found to plays an important regulatory role in stem cell bahaviour (7, 8).

Eph receptors constitute the largest family of receptor tyrosine kinases, and their ligands, ephrins, are glycophophatidylinositol-linked (ephrinA1-10) or transmembrane (ephrinB1-3) proteins. Ephrin ligands bind to the Eph receptors (EphA1-8 and EphA10; EphB1-4 and EphB6) on the apposing cell membrane to initiate bidirectional juxtacrine signalling. In Eph forward signalling, ephrin-induced Eph activations leads to phosphorylation of the cytoplasmic tyrosine kinase domain, whereas in ephrin reverse signalling, Eph receptors triggers several tyrosine residues from ephrinB cytoplasmic domain (9). Eph receptors are classified into two subclasses: EphAs and EphBs, based on their structural similarities and binding affinities to their ligands ephrinA or ephrinB (10).

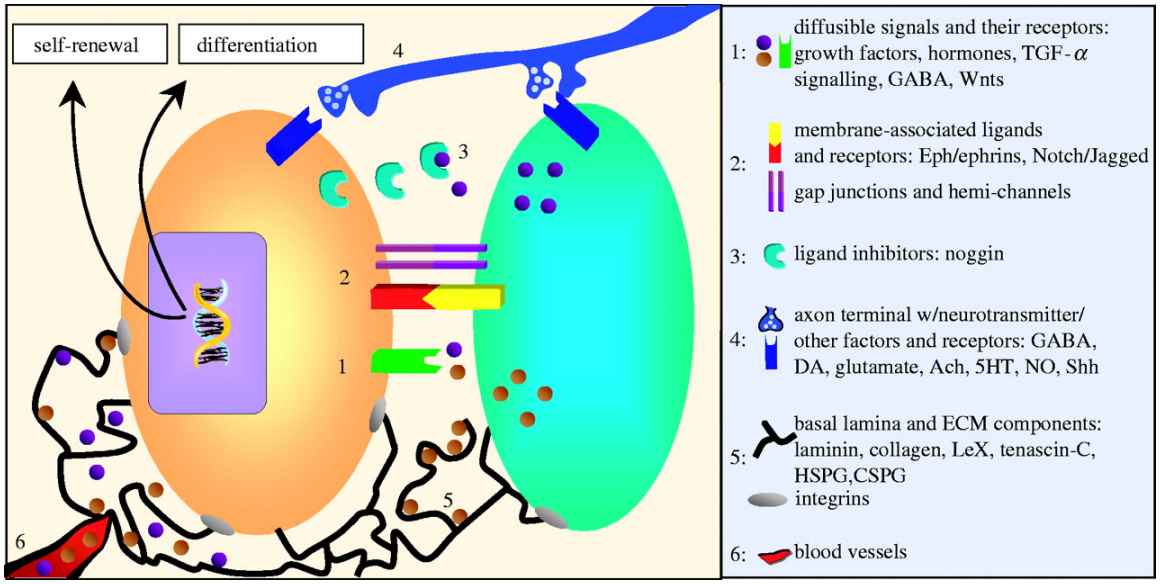

Figure 1.1. Components of the neural stem cell niche (11).

Eph-ephrin signalling coordinates cell-cell interactions in many developing processes, as well as homeostasis and physiology of many adult organs (12, 13). In the central nervous system, Eph receptors and ephrin ligands show complementary patterns of expression in many developing regions. Eph receptor bi-directional signalling plays a critical role in governing axon guidance, cell migration, and topographic mapping (14-16). Furthermore Eph-ephrin signalling has been investigated as a means of regulating neural stem/progenitor cells in proliferation, migration, and survival both during development and in adulthood (10, 17-20). For example, EphA-ephrinA signalling promotes neurogenesis in embryonic telencephalic NSC (21), and ephrinA2-EphA7 reverse signalling negatively regulates neural progenitor cell proliferation in adult SVZ (22). EphB3-ephrinB3 signalling exerts an inhibitory role in NSCs proliferation in the developing SVZ (23), whereas EphB1-ephrinB3 regulates the proliferation and migration of neural progenitors in hippocampus (18).

Till recently, studies have demonstrated that Eph signalling can also regulate NSCs differentiation. In particular, EphB4 receptors and ephrinB2 ligands are primarily expressed by neural stem cells and astrocyte, respectively, and their signalling promotes neuronal differentiation in hippocampus (8, 24). In the SGZ of the hippocampal dentate gyrus, EphB4 receptors are found on hippocampal NSCs, and ephrinB2 ligands are expressed on the cell surface of neighbouring cells astrocytes. EphrinB2 is the sole ligand for EphB4, but ephrinB2 can bind several Eph receptors, including EphB2, EphB4, EphA3, and EphA5 (25). Crystal structures and solution studies have shown that ephrinB2

binds EphB4 receptor to form heterodimer, and their signalling activation requires further formation of higher order clusters by the assembly of Eph-ephrin tetramers into multivalent oligomers (26).

In prior studies, activation of Eph-ephrin signalling was induced by antibody pre-clustered ephrin ligands or Eph receptors in solution, or immobilising ligands on solid surface or beads to artificially generate the multivalent ligand-receptor complexes (27-29). However, these methods are not able to display the physical microenvironment of cell-cell interfaces, because both Eph receptors and ephrin ligands are membrane bound, Eph-ephrin signalling is cell-cell contact dependent (9). With little known about the biophysical mechanisms in Eph-ephrin clustering, it is critical to understand the precise control of the multi-valency and spatial organisaiton of the Eph receptors and their cognate ligands in modulating signalling activation and cellular outcome.

Section 1.2: Spatial organisation of Eph receptor signalling on supported lipid bilayers

The spatial organisation of transmembrane receptors plays a crucial role in signal transduction in living cells, which directs the communication between adjacent cells and their surrounding microenvironment. Membrane receptor-mediated signalling is highly complex. Transmembrane receptors can undergo homotypic and heterotypic cis-interactions as well as intercellular trans-interactions with receptors and/or ligands to form signalling complexes. These signalling complexes are the initiator for downstream signalling events. Many of the receptors do not function as individual signalling units, and their activation requires the formation of higher order clusters that contain hundreds and thousands of receptor-ligand complexes. Examples include T-cell receptors (TCRs), epidermal growth factor receptors (EGFRs), Eph receptors in mammalian cells, and chemotaxis receptors in bacteria (11, 30-36). Studies have shown that the geometric arrangement and physical interactions of membrane-bound receptors can alter signaling processes. In T-cell biology, spatially reorganised immunological synapses can alter TCR signalling (37). In cancer biology, the size and the physical organisation of Eph receptor-ligand clusters can alter the distribution of downstream signalling effectors and cellular outcome (38, 39).

Eph receptors and their ligands ephrin signal juxtacrine. Eph-ephrin signalling is initiated by the direct interaction of membrane bound receptors and ligands. Eph receptors are an exclusive class of receptor tyrosine kinases for

which signalling activation requires not only the dimerisation of the receptors and ligands, but also additional multivalent oligomerisation and higher order clustering of the receptor-ligand complex as crucial prerequisites (40). Because of the dynamic and physiological nature of Eph clustering, it is crucial to understand how cluster size and spatial organisation modulate signalling outcome. A supported lipid bilayer is a well-suited system for studying membrane receptor-ligand associated signalling. It reconstitutes the physical geometry and chemical composition of Eph-ephrin signalling. Mechanical properties and spatial organisation of cell surface receptors are increasingly recognised as relevant cellular stimuli [12-14]. Studies have revealed physical force sensing of EphA receptors could modulate intracellular signalling cascades that in turn alters cellular behaviour. When EphA2 receptor movement was restricted by mechanical forces, the formation of receptor-ligand cluster was reorganised, this resulted a change in proximal membrane signalling events (38, 39). This suggests the possibility that EphB signalling is also spatio-mechanosensitive, since EphA and EphB receptors share similarities in their physical structures and ligand interactions. Altogether, these results motivate the hypothesis that neural stem cell differentiation may be regulated by EphB signalling in response to the receptor-ligand spatial re-organisation.

Prior studies have used synthetic dimeric ephrinB2-Fc fusion proteins or engineered polymer chains to artificially precluster ephrin ligands in solution to activate EphB4 signalling [(8, 24). In my thesis study we designed and expressed a monomeric form of ephrinB2 ligands that can manipulate the natural clustering occurrence of Eph receptor and ephrin ligand on a supported lipid membrane. In particular, we reconstituted a hybrid system to mimic the physical geometry and the chemical composition of the Eph-ephrin signalling. Living NSCs expressing EphB4 receptors interact with the apposing membrane displaying laterally mobile ephrinB2 ligand on a glass support. This setup also accommodates spatial mutations, which is the orchestrated mechanical disruption of the spatial patterning of proteins on the lipid bilayer. Spatial mutations are implemented by nano-fabricating chromium (Cr) structures on the glass substrate, which serve as diffusion barriers inhibiting receptor-ligand diffusion, which in turn also controls the cluster size and number of receptor-ligand complexes (41). Previous studies have suggested that the density of Ephs and ephrins on the cell surface may directly influence the signalling outcome, likely by impacting on the size and stability of signalling clusters. The mechanism by which EphB4-ephrin2 interaction transduces mechanical signals to downstream biochemical changes remains unknown. We hypothesize that spatial organisation of cell surface receptors is crucial for mechanotransduction, force modulation that disrupts the mechanochemical coupling may represent a critical step in neurogenesis. Specifically, mechanical ligand restriction extends to the spatial organisation of

EphB4 receptor at cell surface junctions and alters the cellular response to ephrinB2, which in turn neuronal differentiation can be modulated.

Section 1.3: Chapter 1 references

1. Fuentealba LC, Obernier K, & Alvarez-Buylla A (2012) Adult neural stem cells bridge their niche. *Cell stem cell* 10(6):698-708.
2. Ming GL & Song H (2011) Adult neurogenesis in the mammalian brain: significant answers and significant questions. *Neuron* 70(4):687-702.
3. Keung AJ, Kumar S, & Schaffer DV (2010) Presentation counts: microenvironmental regulation of stem cells by biophysical and material cues. *Annual review of cell and developmental biology* 26:533-556.
4. Shawdee Eshghi DVS (2008) Engineering microenvironments to control stem cell fate and function. *StemBook*.
5. Keung AJ, de Juan-Pardo EM, Schaffer DV, & Kumar S (2011) Rho GTPases mediate the mechanosensitive lineage commitment of neural stem cells. *Stem cells* 29(11):1886-1897.
6. Saha K*, et al.* (2008) Substrate modulus directs neural stem cell behavior. *Biophysical journal* 95(9):4426-4438.
7. Koch U, Lehal R, & Radtke F (2013) Stem cells living with a Notch. *Development* 140(4):689-704.
8. Ashton RS*, et al.* (2012) Astrocytes regulate adult hippocampal neurogenesis through ephrin-B signaling. *Nature neuroscience* 15(10):1399-1406.
9. Himanen JP, Saha N, & Nikolov DB (2007) Cell-cell signaling via Eph receptors and ephrins. *Current opinion in cell biology* 19(5):534-542.
10. Genander M & Frisen J (2010) Ephrins and Eph receptors in stem cells and cancer. *Current opinion in cell biology* 22(5):611-616.
11. Riquelme PA, Drapeau E, & Doetsch F (2008) Brain micro-ecologies: neural stem cell niches in the adult mammalian brain. *Philosophical transactions of the Royal Society of London. Series B, Biological sciences* 363(1489):123-137.
12. Pasquale EB (2005) Eph receptor signalling casts a wide net on cell behaviour. *Nature reviews. Molecular cell biology* 6(6):462-475.
13. Yamaguchi Y & Pasquale EB (2004) Eph receptors in the adult brain. *Current opinion in neurobiology* 14(3):288-296.
14. Goldshmit Y, McLenachan S, & Turnley A (2006) Roles of Eph receptors and ephrins in the normal and damaged adult CNS. *Brain research reviews* 52(2):327-345.
15. Klein R (2012) Eph/ephrin signalling during development. *Development* 139(22):4105-4109.
16. Murai KK & Pasquale EB (2003) 'Eph'ective signaling: forward, reverse and crosstalk. *Journal of cell science* 116(Pt 14):2823-2832.
17. Genander M*, et al.* (2009) Dissociation of EphB2 signaling pathways mediating progenitor cell proliferation and tumor suppression. *Cell* 139(4):679-692.

18. Chumley MJ, Catchpole T, Silvany RE, Kernie SG, & Henkemeyer M (2007) EphB receptors regulate stem/progenitor cell proliferation, migration, and polarity during hippocampal neurogenesis. *The Journal of neuroscience : the official journal of the Society for Neuroscience* 27(49):13481-13490.
19. Holmberg J*, et al.* (2005) Ephrin-A2 reverse signaling negatively regulates neural progenitor proliferation and neurogenesis. *Genes & development* 19(4):462-471.
20. Nomura T, Goritz C, Catchpole T, Henkemeyer M, & Frisen J (2010) EphB signaling controls lineage plasticity of adult neural stem cell niche cells. *Cell stem cell* 7(6):730-743.
21. Aoki M, Yamashita T, & Tohyama M (2004) EphA receptors direct the differentiation of mammalian neural precursor cells through a mitogen-activated protein kinase-dependent pathway. *The Journal of biological chemistry* 279(31):32643-32650.
22. Doerks T, Copley RR, Schultz J, Ponting CP, & Bork P (2002) Systematic identification of novel protein domain families associated with nuclear functions. *Genome research* 12(1):47-56.
23. del Valle K, Theus MH, Bethea JR, Liebl DJ, & Ricard J (2011) Neural progenitors proliferation is inhibited by EphB3 in the developing subventricular zone. *International journal of developmental neuroscience : the official journal of the International Society for Developmental Neuroscience* 29(1):9-14.
24. Conway A*, et al.* (2013) Multivalent ligands control stem cell behaviour in vitro and in vivo. *Nature nanotechnology* 8(11):831-838.
25. Diehl S*, et al.* (2005) Altered expression patterns of EphrinB2 and EphB2 in human umbilical vessels and congenital venous malformations. *Pediatric research* 57(4):537-544.
26. Chrencik JE*, et al.* (2006) Structural and biophysical characterization of the EphB4*ephrinB2 protein-protein interaction and receptor specificity. *The Journal of biological chemistry* 281(38):28185-28192.
27. Wimmer-Kleikamp SH, Janes PW, Squire A, Bastiaens PI, & Lackmann M (2004) Recruitment of Eph receptors into signaling clusters does not require ephrin contact. *The Journal of cell biology* 164(5):661-666.
28. Wimmer-Kleikamp SH, Janes PW, Squire A, Bastiaens PIH, & Lackmann M (2004) Recruitment of Eph receptors into signaling clusters does not require ephrin contact. *The Journal of cell biology* 164(5):661-666.
29. Lin KT, Sloniowski S, Ethell DW, & Ethell IM (2008) Ephrin-B2-induced cleavage of EphB2 receptor is mediated by matrix metalloproteinases to trigger cell repulsion. *The Journal of biological chemistry* 283(43):28969-28979.
30. Keppler A*, et al.* (2003) A general method for the covalent labeling of fusion proteins with small molecules in vivo. *Nature biotechnology* 21(1):86-89.

31. Hartman NC, Nye JA, & Groves JT (2009) Cluster size regulates protein sorting in the immunological synapse. *Proceedings of the National Academy of Sciences of the United States of America* 106(31):12729-12734.
32. Moran U, Phillips R, & Milo R (2010) SnapShot: key numbers in biology. *Cell* 141(7):1262-1262 e1261.
33. Dustin ML & Groves JT (2012) Receptor signaling clusters in the immune synapse. *Annual review of biophysics* 41:543-556.
34. Davis S (1994) Ligands for EPH-Related ReScience 97 receptor Tyrosine Kinases That Require Membrane Attachment or Clustering for Activity. *Science* 266(No. 5186):816-819.
35. Hilmanen JP (2010) Architecture of Eph receptor clusters. *PNAS* 107(no.24):10860-10865.
36. Chan YH, van Lengerich B, & Boxer SG (2009) Effects of linker sequences on vesicle fusion mediated by lipid-anchored DNA oligonucleotides. *Proceedings of the National Academy of Sciences of the United States of America* 106(4):979-984.
37. Kaspar D. Mossman GC, Jay T. Groves, Michael L. Dustin. (2005) Altered TCR Signaling from Geometrically Repatterned Immunological Synapses. *Science* 310(5751):1191-1193.
38. Greene AC*, et al.* (2014) Spatial organization of EphA2 at the cell-cell interface modulates trans-endocytosis of ephrinA1. *Biophysical journal* 106(10):2196-2205.
39. Salaita K*, et al.* (2010) Restriction of receptor movement alters cellular response: physical force sensing by EphA2. *Science* 327(5971):1380-1385.
40. Bethani I, Skanland SS, Dikic I, & Acker-Palmer A (2010) Spatial organization of transmembrane receptor signalling. *The EMBO journal* 29(16):2677-2688.
41. Nair PM, Salaita K, Petit RS, & Groves JT (2011) Using patterned supported lipid membranes to investigate the role of receptor organization in intercellular signaling. *Nature protocols* 6(4):523-539.

Chapter 2

Section 2.1: Design and functionalisation of ephrinB2 ligands on supported lipid bilayers

The central platform of my thesis research is a hybrid system that reconstitutes the juxtacrine signalling geometry between live neural stem cells expressing EphB4 receptors and supported lipid membranes displaying laterally mobile monomeric ephrinB2 ligands. This system provides a physiologically relevant microenvironment for studying the interaction between membrane bound receptor and ligand in cell-cell communication. It also allows us to precisely control the chemical composition of the ligands and the membranes, as well as the spatial distribution of receptor-ligand complexes using the technique of spatial mutation.

The development of an appropriate and feasible biochemical conjugation method for tethering ephrinB2 ligand on the supported bilayer is critical for this setup. Because we are interested in studying the effect of membrane bound ephrinB2 induced signalling in neural stem cell function, and differentiation studies typically are carried out in a course of 5 days *in vitro*. For this reason, we needed to establish a secure chemical linkage between the phospholipid bilayer and the protein ligands, to assure an uninterrupted engagement of ephrinB2 ligands and Eph receptors on NSCs membrane. Many of the commonly used protein-bilayer chemical linkages are not sufficient for this task. For example, nickel-chelating lipids bind to histidine-tagged proteins, but this linkage is labile for a 5-day cell culture condition. In particular, nickel-chelation reaction is quite sensitive to temperature (differentiation culture is typically in 37 °C), and the reaction undergoes dissociation in hours (1). In addition, we have found that nickel-chelation chemistry is not compatible with the NSCs cell culture medium. Specifically there are assorted metal ions in the medium that may compete with nickel-histidine reaction, causing dissociation. When we incubated cell culture medium on nickel-funtionalised supported lipid bilayer, histidine-tagged ephirnB2 protein dissociated within 30 minutes (results not shown). Another commonly used biochemical crosslink method is the maleimide-thiol reaction, whereby maleimide funtionalised lipids form covalent bonds with the thiol groups

on cysteine residues of a protein. However, this reaction requires high concentrations of ephrinB2 proteins. Typically, mammalian expressed ephrinB2 proteins produce relatively low yield. Therefore the maleimide-thiol crosslink is not efficient for this manner. Biotin, avidin, and streptavidin linkages have been known as the strongest non-covalent interactions. The formation between biotin and avidin is rapid and unaffected by extremes of pH, temperature, organic solvents and other denaturing agents. However this method can introduce artificial clusters. In particular, it can cause ligands to aggregate and form preclusters due to the multiple binding sites on streptavidin (2). To obviate these problems, we require that a suitable linker should bear NSCs culture medium at 37 °C, maintain monomeric form of ephrinB2 ligand, and be sufficiently stable to study 5-day differentiation.

DNA oligonucleotides are a popular means to assemble protein molecules because anti-parallel hybridised DNA molecules are known to be highly specific and sensitive. There are various methods for cross-linking oligonucleotides with protein: disulfide formation between DNA templates and their binding proteins, click chemistry by azide and alkyne groups, photo-induced cross-linking (3, 4), oxidative cross-linking (5), and hydrogen bonding formation (6). Moreover, DNA molecules have been incorporated into liposomes and supported membranes for studying DNA mediated vesicle fusion (7-9). DNA oligonucleotides can also be anchored to the lipid membrane of a cell surface to study cell adhesion on solid surface (10, 11). More recently, studies have demonstrated the use of DNA oligonucleotides for directing ligand oligomerisation and formation of protein heterodimers (12).

These DNA oligonucleotides based conjugations and incorporation applications in biological and chemical systems encouraged us to develop a method based on DNA-protein crosslinking to functionalise ephrinB2 ligands on the supported lipid membrane in an efficient and stable manner. SNAP-tag, a 20kDa mutant of DNA repair protein O^6-alkylguanine-DNA alkyltransferase has been used as a versatile fusion protein that performs a site-specific irreversible covalent reaction with a benzylguanine (BG) substrate (13, 14). A complementary set of 20 base pair DNA oligonucleotides was used to link ephrinB2 ligands and the supported membrane. One strand of DNA was conjugated to ephrinB2 ligand, and the other was linked with lipid head group molecules on supported membrane. Applying the advantages of these versatile biochemical reactions, we designed a three-step conjugation to anchor ephrinB2 ligand on supported lipid bilayer. First, monomeric ephrinB2 ligand was genetically fused with SNAP-tag protein and then ephrinB2-SNAP fusion protein can be conjugated with a single stranded DNA (sequence1) with benzylguanine (BG) and Cy5 modifications to form a fluorescent DNA-ephrinB2 ligand complex. Second, a thiol-group modified complementary DNA (sequence2) was functionalised to a maleimide lipid bilayer;

third, DNA (sequence1)-ephrinB2 complex was tethered onto the bilayer through DNA-hybridisation with its complementary thiol-DNA (sequence2) (Figure 2.1.). This method accommodates efficient and stable reactions between DNA, protein, and bilayer. Furthermore, we tested the functional role of ephrinB2 ligands with NCSs on the lipid bilayer in various fluorescent microscopic experiments, which I discuss in the next section.

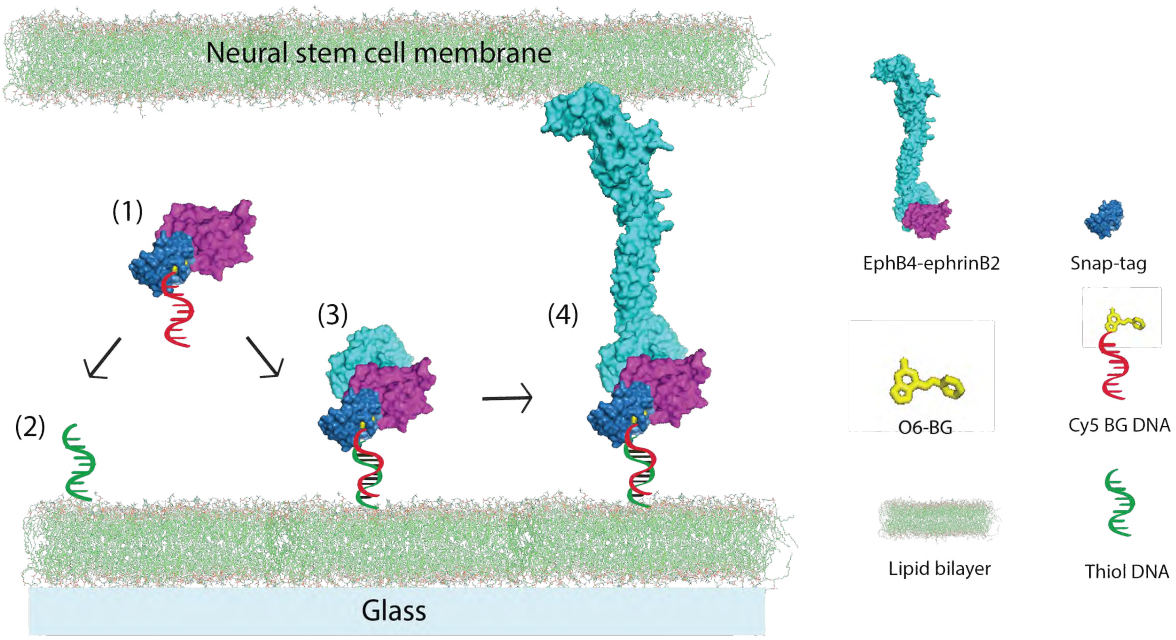

Figure 2.1: Schematic of experimental setup: a hybrid system with NSCs expressing EphB4 receptors on the cell membrane and ephrinB2 ligands displaying on a supported lipid bilayer. (1) EphrinB2-SNAP tag fusion protein was conjugated with Cy5-BG modified single stranded DNA. (2) Thiol-modifed single stranded DNA was functionalised with maleimide decorated DOPE lipid bilayer. (3) EphrinB2-DNA complex reacted with thiol-DNA through complementary DNA sequence hybridisation. (4) NSCs expressing EphB4 receptors were deposited on supported lipid bilayer and binding with ephrinB2 ligands.

Section 2.2: Formation and characterisation of DNA-ephrinB2 based bilayer

A supported lipid bilayer was constructed via spontaneous self-assembly of phospholipids on a hydrophilic glass substrate (2). Small unilamellar vesicles (SUVs) composed of 1:20 molar ratio of maleimide functionalised DOPE to DOPC (see experimental section for details) were assembled into a lipid bilayer on a glass substrate support. Thiolated single stranded DNA (sequence2) was functionalised to the supported lipid bilayer through maleimide DOPE. Monomeric ephrinB2 ligands conjugated with Cy5 fluorescently labeled single stranded oligonucleotides (sequence1) were tethered onto a supported lipid bilayer through DNA-DNA hybridisation as previously described. Epifluorescence images of cy5 labeled DNA-ephrinB2 ligands on supported lipid bilayer revealed homogeneous distribution of the ligands. The fluidity of the bilayer as well as the mobility of the ligands were confirmed by fluorescence recovery after photo bleaching (FRAP) experiments (Figure 2.2.). Furthermore we used fluorescence correlation spectroscopy (FCS) analysis to determine the density and diffusion coefficient of ephrinB2 ligands on the supported lipid bilayer. A typical time autocorrelation function of fluorescence intensity fluctuations from membrane bound ephrinB2 is shown in Figure 2.3. In the FCS experiments, we tested the ligand surface densities of two solution concentrations of ephrinB2: 20 nM and 100 nM, respectively. The results we obtained from the FCS measurement showed similar values of the surface ligand density of both ephrinB2 ligands solution concentrations. We observed ephrinB2 ligand density of 120/μm^2 with a diffusion coefficient of 4.0 $\mu m^2/s$. This result is typical for lipid diffusion on supported membranes (15, 16).

We have successfully developed a biochemical coupling method for tethering ephrinB2 ligands on supported lipid bilayer. This tool has provided stable attachment of the ligands on bilayer for hours, as was confirmed from fluorescent intensity measurements of ephrinB2 ligands on the bilayer. We took epifluorescent images of ephrinB2 ligands every two hours, and we found that there was no significant changes in the fluorescent intensity. These results indicated that the ephrinB2 ligands did not dissociate over this time period. This biochemical conjugation method allowed us to study Eph-ephrin signalling on supported lipid bilayer for days. In particular we were able to investigate how spatial and mechanical manipulation of receptor-ligand organisation can regulate NSCs differentiation.

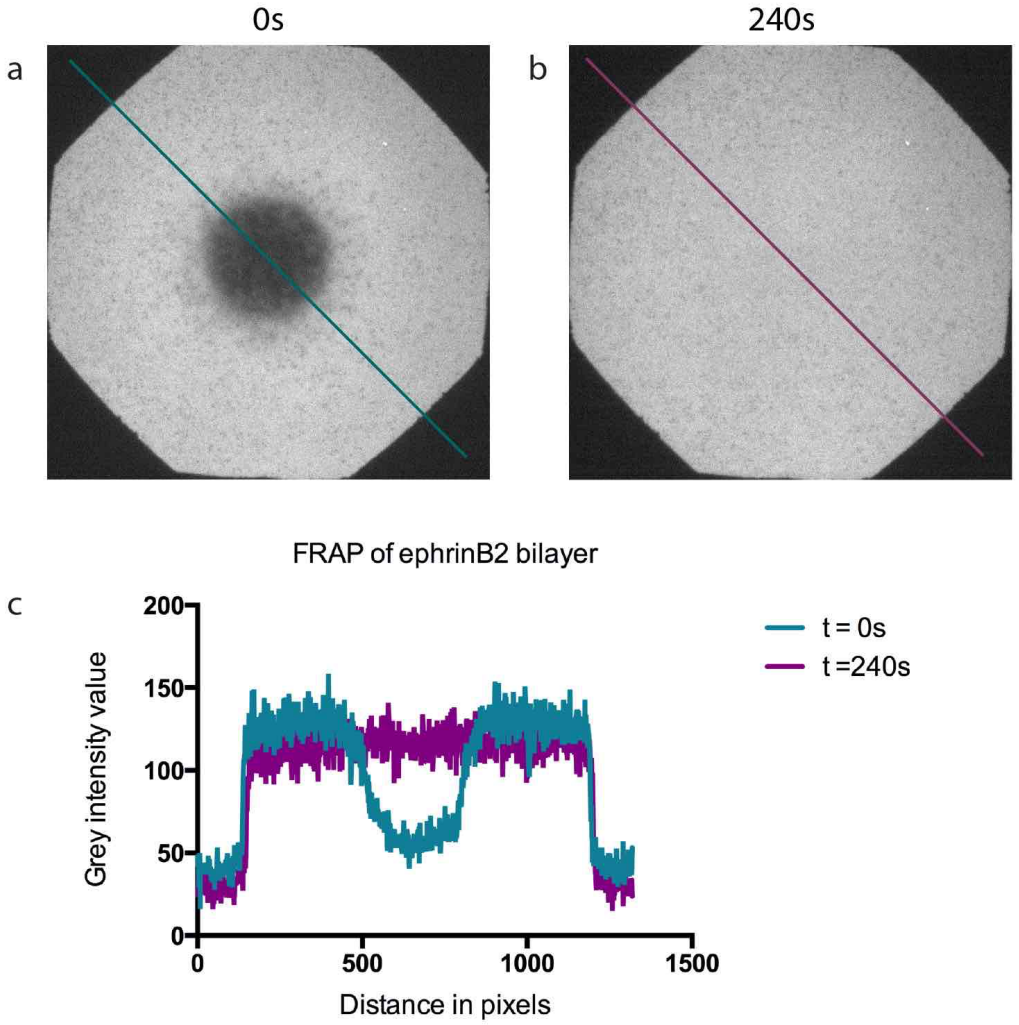

Figure 2.2. Fluorescence recovery after photobleaching (FRAP) of ephrinB2 displaying supported lipid bilayer. a. A region of the bilayer was bleached for 1 minute with 647 nm epifluorescent lightsouce. Images were captured every 30 seconds after photobleaching, with images at 0 second and 240 seconds presented here. b. Fluorescent density analysis of a line scale confirmed the fluidity of the supported lipid bilayer. Bilayer fluorescence was recovered after 240 seconds.

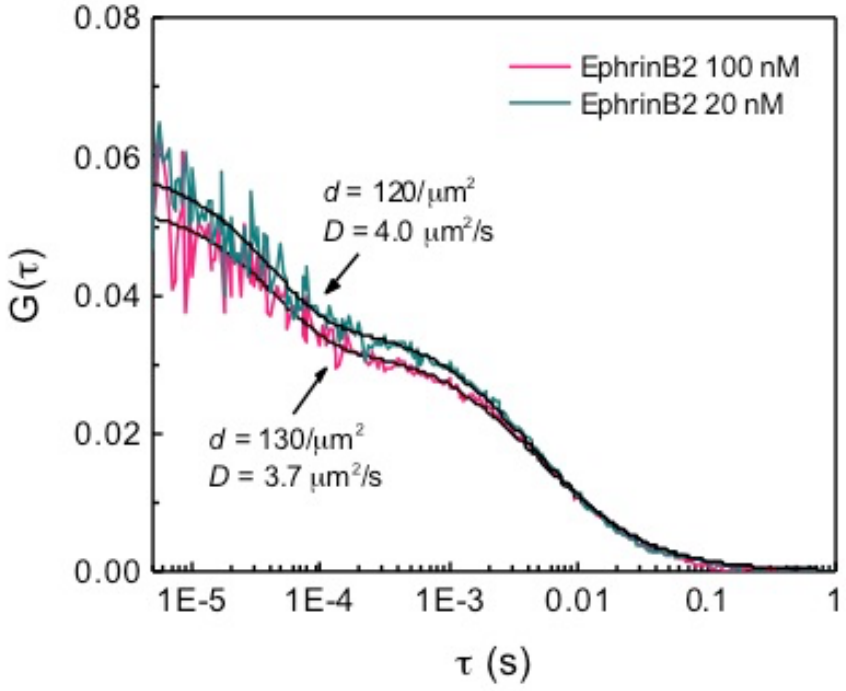

Figure 2.3. Fluorescence correlation spectroscopy (FCS) revealed ephrinB2 ligands density on the supported lipid bilayer. Measurements were taken of the Cy5 labeled ephrinB2 ligands diffusing on supported membrane.

To achieve the reconstitution of juxtacrine geometry for Eph-ephrin signalling, we cultured neural stem cells on a supported lipid bilayer functionalised with freely diffusing ephrinB2 ligands. Employing total internal reflection fluorescence (TIRF) microscopy to illuminate just the cell-bilayer interface, we recorded in live time NSC clusters on the ephrinB2-presenting bilayer. Time-lapse images demonstrated the spatial distributions and the micro-cluster formation of ephrinB2 with NSCs at the membrane-cell interface. EphrinB2 ligands diffused laterally on a fluid supported membrane and rapidly organised into micro-clusters with NSCs upon cell landing. In the next 45 minutes the cluster continued to travel and form bigger clusters. We observed an inward radial like transport of ephrinB2 ligands and a formation of a centralized cluster after 45 minutes of cell landing (Figure 2.4.).

Images from reflection interference contrast microscopy (RICM) indicated cell adhesion pattern on the membrane-cell interface. Ligand-receptor binding provided the only linker between NSCs and supported lipid bilayer. To confirm this, we cultured neural stem cells on the supported lipid bilayer in the absence of ephrinB2 ligands. In this experiment, cells failed to form adhesion on the

supported membrane, and this result was confirmed by RICM images. It has been revealed that ephrinB2 is the sole ligand for EphB4 receptors, however ephrinB2 can also bind to other Eph receptors, such as EphB2 receptors, which are also expressed on NSCs membrane (17). When we used antibodies to pre-block the EphB2 and EphB4 ligand-binding sites respectively, we observed a decrease in the number of cells that can adhere on ephrinB2 bilayer for both Eph receptor blocking conditions. However pre-blocking EphB4 receptors had more significant inhibitory effects on cell adhesion, suggesting that EphB4 receptors are the predominant binding partner for ephrinB2 ligands. When we blocked both EphB2 and EphB4 receptors, we observed an inhibitory effect on cell adhesion (Figure 2.5.), which suggested that ephrinB2 ligands on the supported lipid bilayer can bind to both EphB2 and EphB4 receptors on NSCs. To further confirm that the formation of ephrinB2 micro-clusters on the supported lipid bilayer was the result of EphB4 receptor binding on NSCs as reported in an earlier study (18), we engineered a stable NSCs cell line that EphB4 receptor was genetically fused with a fluorescent protein mCherry. Applying TIRF and confocal microscopies, we captured fluorescent images demonstrating a co-localisation of EphB4 receptors and ephrinB2 ligands at membrane-cell interface (Figure 2.6.). This co-localisation indicated ephrinB2 ligands cluster was in response to the EphB4 receptors in NSCs.

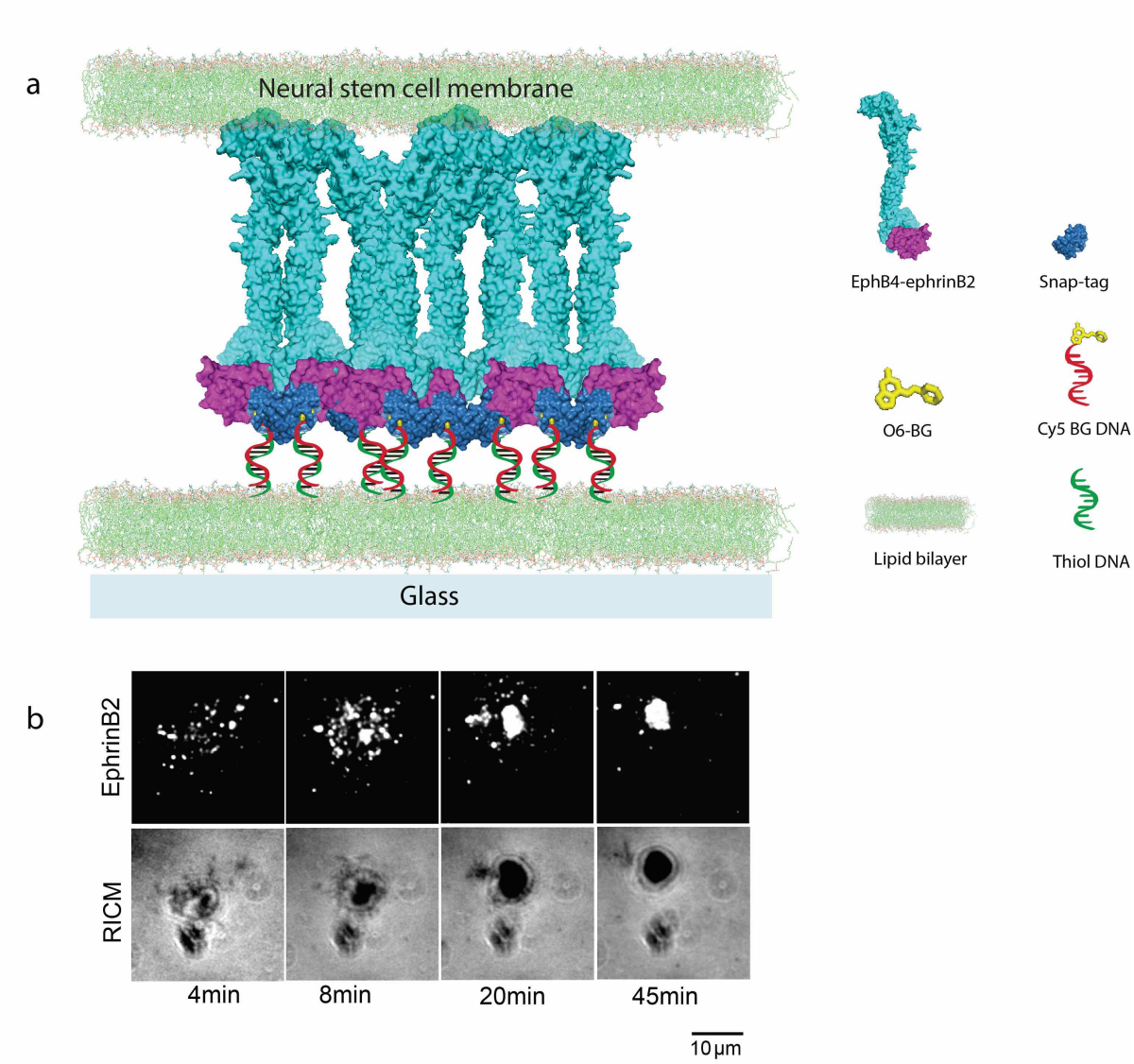

Figure 2.4. Schematic and images of the hybrid live cell-supported membrane system on which ephrinB2 ligands bind and cluster with NSCs. a. Schematic: ephrinB2 ligands diffuse laterally on a supported lipid bilayer to bind and cluster with NSCs on the opposing membrane. b. Image: time-lapse RICM and TIRF images of ephrinB2 ligands formed micro-clusters with NSCs.

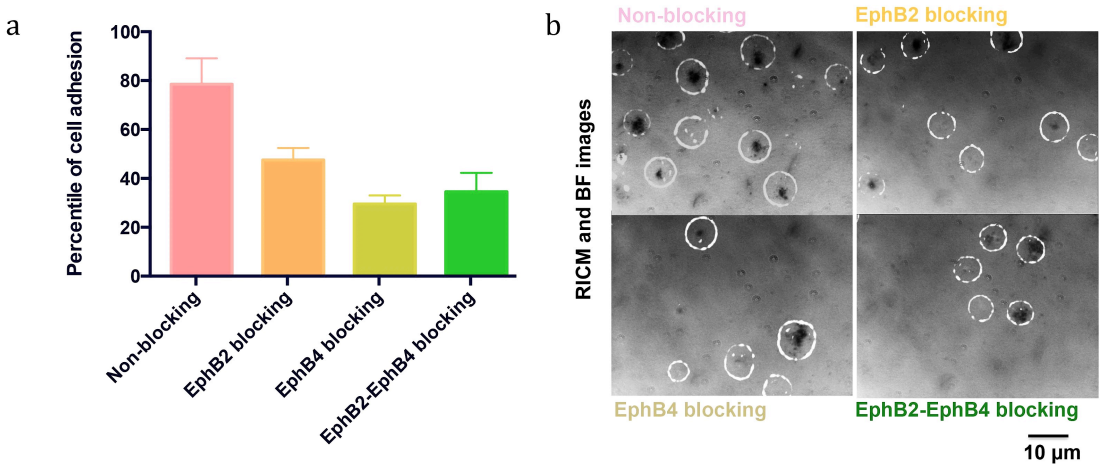

Figure 2.5. Blockage of ephrin ligand binding sites on EphB receptors inhibited NSCs adhesion on ephrinB2 displaying supported membrane. NSCs cells were treated with antibodies that blocked the ephrin binding site on EphB receptors. Antibody treated NSCs were cultured on ephrinB2 bilayer for 30 minutes, RICM and bright field (BF) images were captured afterwards. a. The ratio between number of cells adhered on bilayer (RICM) over number of cells on the bilayer was calculated for quantifying the proportion of cell adhesion. b. Overlay of RICM and BF images of NSCs on ephrinB2 bilayer after 30 minutes of cell attachment. White circles represented bright field images.

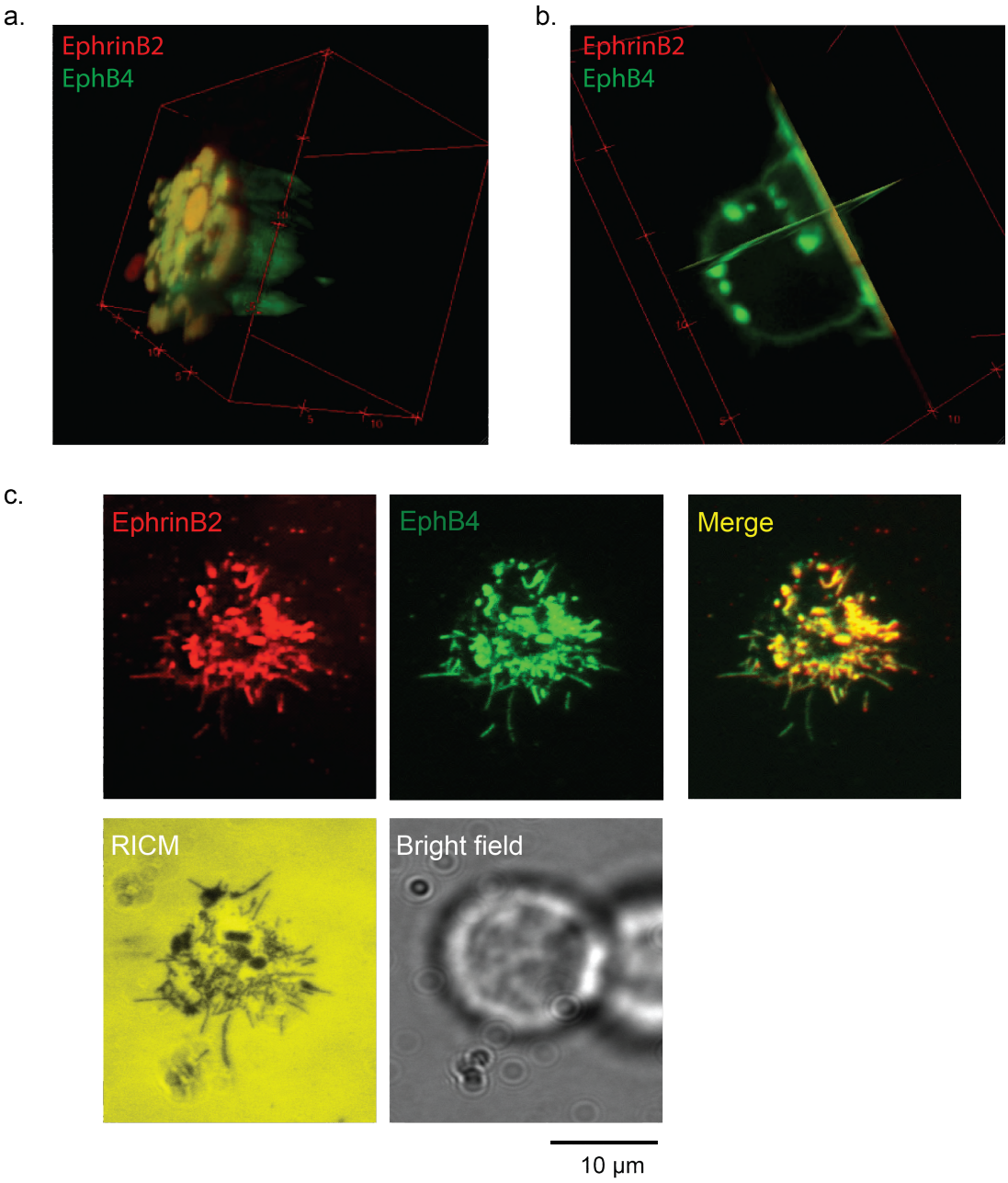

Figure 2.6. Confocal and TIRF images of EphB4 receptors and ephrinB2 ligands co-localisation at the cell-membrane interface. a. A confocal image of a neural stem cell expressing m-cherry-EphB4 receptors cluster with ephrinB2 bilayer. b. A cross-section image of a. c. TIRF, RICM, and bright field images of EphB4 receptors on a NSC surface bind and cluster with ephrinB2 ligands on the apposing membrane. Merged images of ephrinB2 and EphB4 indicated co-localisation of receptor-ligand.

From previous experiments, we have confirmed that Eph-ephrin binding provides the only physical linkage between NSCs and the supported membrane. RICM images confirmed the EphB4-ephrinB2 clusters co-localise with the regions of closest intermembrane contact. To determine if the observed inward radial like transport of ephrinB2 ligands is an indirect consequence of intermembrane anchoring, a cyclic RGD (Arg-Gly-Asp) peptide was introduced into the supported membrane. We conjugated a cyclic RGD peptide with single-stranded DNA oligonucleotides. This RGD tethered DNA served as a binding partner for integrin receptors on the cell surface of NSCs and it was also displayed as a binary mixture with ephrin-B2 ligands on the supported membrane. RGD-DNA was tethered on the supported lipid bilayer through DNA-DNA hybridisation. We applied a similar concept to biochemically crosslink the single stranded DNA oligonucleotides and RGD peptide as DNA-ephrinB2 complex (Figure 2.7.).

In this setup, RGD-DNA was introduced to assist cell spreading and adhesion. The ligand density of RGD-DNA required on bilayer surface had to be maintained at an optimal level to efficiently generate enough adhesion area without interfering with EpB4 receptor signalling. We titrated the RGD peptide density and carefully examined the cell adhesion patterns at cell-bilayer interface using RICM imaging. We found that a condition of molar ratio at 1:20 of RGD peptide to ephrinB2 ligand offered optimal results. We also measured ligand densities of both RGD-DNA and ephrinB2-DNA in the binary bilayer by FCS. FCS results revealed that RGD-DNA and ephrinB2-DNA ligands had similar densities and diffusion coefficients.

NSCs were cultured on RGD : ephrinB2 binary bilayer for 45 minutes to permit complete formation of RGD-integrin binding as well as ephrinB2-EphB4 clustering. Fluorescent images revealed the binding pattern of RGD peptides as well as ephrinB2 ligands. Interestingly, we observed an altered morphology of ephrinB2-EphB4 organisation in the presence of RGD peptides. RICM images showed that NSCs spread uniformly and formed large contact areas at the interface of cell-bilayer in the presence of RGD. EphrinB2-EphB4 no longer organised into a centralised cluster, in contrast with what we observed in the absence of RGD. Instead, ephrinB2-EphB4 formed scattered micro-clusters that co-localised with the closest contact area at membrane interface. RGD-integrin focal adhesion formed a ring structured morphology surrouding the ephrinB2-EphB4 clusters, and did not colocalise with ephrinB2-EphB4. Thus, we conclude that the radial transport of EphB4 we observed earlier might be a passive diffusion process, specifically ephrinB2 ligands cluster with EphB4 receptors through indirect intermembrane anchoring. Previously, EphA2 receptors have been shown to undergo active clustering, and the presence of RGD peptide did not alter the EphA2 cluster organisation, and it still formed a centralised structure (19). Our new observations on EphB4 receptors suggest that EphA and EphB

receptors cluster differently with their membrane bound monomeric ephrin ligands. This motivated us to continue to investigate if biophysical manipulation on receptor-ligand spatial organistion can affect EphB4 signalling in NSCs.

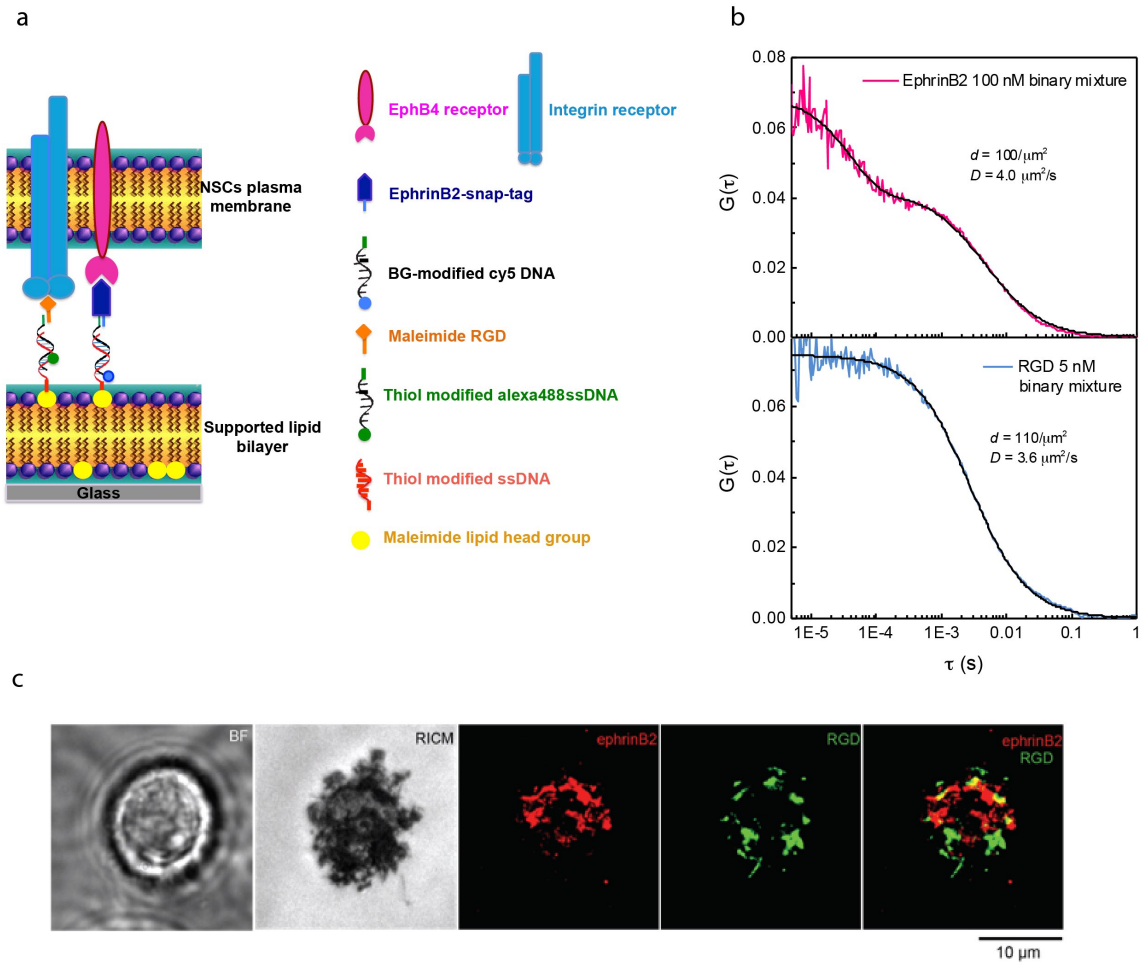

Figure 2.7. RGD : ephrinB2 binary supported membrane. a. Schematic of RGD : ephrinB2 binary supported membrane interacts with cell surface receptors on apposing membrane. RGD peptides bind to integrin receptors on NSCs; whiles ephrinB2 ligands bind to EphB4 receptors on NSCs. b. FCS data shown RGD molecules and ephrinB2 molecules diffuse laterally on a binary supported membrane. EphrinB2 ligands displayed on the supported membrane with a ligand density of 100/μm², and a diffusion coefficient of 4.0 μm²/s. RGD molecules displayed on the supported membrane with a molecular density of 110/μm², and a diffusion coefficient of 3.6 μm²/s. c. Bright field, RICM, and epifluorescent images of a neural stem cell binding to RGD : ephrinB2 displaying bilayer.

Section 2.3: Materials and Methods

Protein expression and purification

The gene encoding sequence of mouse ephrinB2-extracellular domain was cloned into a pFastBac vector containing the SNAP tag and His10 sequences (Figure 2.8.) (pFastBac vector was obtained as a gift from of Kate Alfelri, Groves Lab, UC Berkeley, CA). The cloning vector was then introduced into DH10Bac™ *E. coli* cells to form a recombinant expression bacmid using Bac-to-Bac® baculovirus expression system (Invitrogen). The recombinant bacmid was then used to transfect SF9 insect cells (SF9 cells were obtained from Ann Fischer, UC Berkeley, CA). EphrinB2-SNAP tag-His10 fusion protein was secreted from transfected SF9 cells. SF9 cell culture was precipitated via centrifugation, and supernatant containing EphrinB2-SNAP tag-His10 was collected and purified using a gravity flow column containing Ni^{2+}-NTA resin (Qiagen, Valencia, CA), and eluted using an imidazole gradient. Purified protein was separated by polyacrylamide gel electrophoresis and stained, and a band at molecular weight of 47.759 kDa was detected (Figure 2.8.).

a

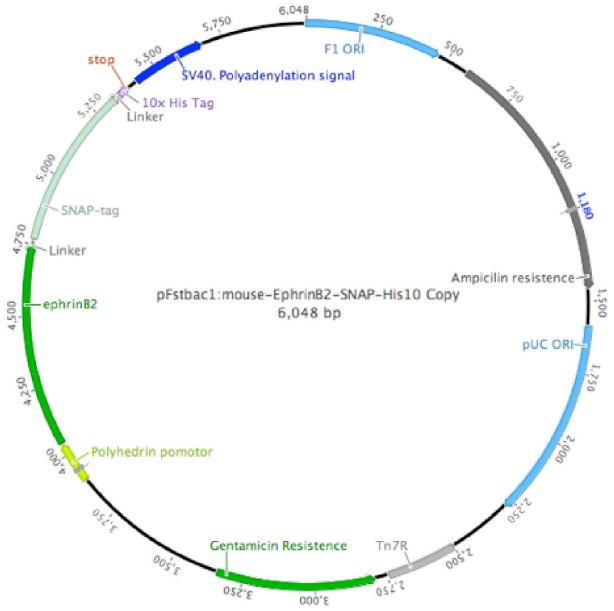

c

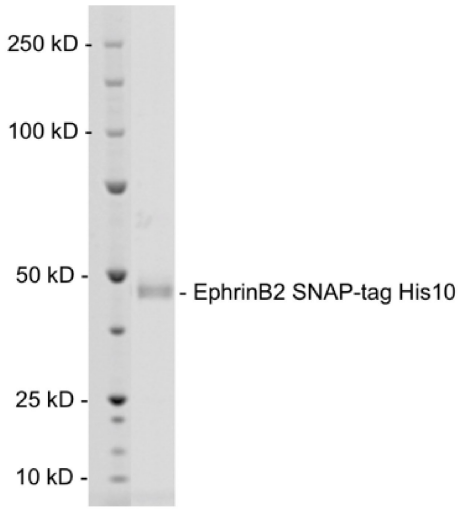

b

MAMARSRRDSVWKYCWGLLMVLCRTAISRSIVLEPIYWNSSNSKFLPGQGLVLYPQIGD
KLDIICPKVDSKTVGQYEYYKVYMVDKDQADRCTIKKENTPLLNCARPDQDVKFTIKFQ
EFSPNLWGLEFQKNKDYYIISTSNGSLEGLDNQEGGVCQTRAMKILMKVGQDASSAGSA
RNHGPTRRPELEAGTNGRSSTTSPFVKPNPGSSTDGNSAGHSGNNLLGSEGGSGGSAAA
CRLVMDKDCEMKRTTLDSPLGKLELSGCEQGLHRIIFLGKGTSAADAVEVPAPAAVLGG
PEPLMQATAWLNAYFHQPEAIEEFPVPALHHPVFQQESFTRQVLWKLLKVVKFGEVIS
YSHLAALAGNPAATAAVKTALSGNPVPILIPCHRVVQGDLDVGGYEGGLAVKEWLLAH
EGHRLGKPGLGALEGGSGGSHHHHHHHHHH

Figure 2.8. Engineering and expressing an EphrinB2 SNAP-tag fusion protein. a. pFASTBac vector containing EphrinB2 SNAP-tag His10. b. Amino acid sequence of mouse monomeric ephrinB2 fusion protein consisting of the soluble portion of extracellular domain (green) linked to SNAP-tag fusion protein (yellow) with a His10-tag (pink) sequence on the C-terminus. c. SDS-PAGE gel electrophoresis with Sypro Ruby stain confirmed success expression and purification of ephrinB2-SNAP tag His10 fusion protein showing a black band at molecular weight of 47.76 kDa.

Preparation of Benzylguanine (BG) modified DNA

The following DNA sequence was used (11, 12):

Sequence1: (seq1): 5'– CCC TAG AGT GAG TCG TAT GA – 3'

DNA oligonucleotides with seq1 modifications described next were purchased from Integrated DNA Technologies (Coralville, IA). These DNA oligonucleotides were modified with an amino modifier C6 on the 5' end of the strand, and a Cy5™-Sp modifier on the 3' end of the strand and purified by HPLC. NH2.seq1.Cy5 were dissolved in TE buffer to a concentration of 5mg/ml and they were precipitated in ethanol. After ethanol precipitation, DNA oligonucleotides were rehydrated in distilled water and stored in -20 °C before further modification.

BG-HNS-GLA was purchased from New England Biolabs (Ipswich, MA), and was dissolved in anhydrous *N, N'*-dimethylformamide (DMSO) (Solulink, CA) to obtain 50 mM concentration. BG-NHS-GLA was reacted with 25 times molar mass equivalent of NH2.seq1.Cy5 at room temperature for 2 hours, and the reaction was kept in 4 °C overnight. The next day, the reaction was analysed by Matrix-assisted laser desorption/ionisaton (MALDI) mass spectrometry. A peak of modified mass intensity change on MALDI analysis confirmed the completion of the reaction (Figure 2.9.). Reaction was desalted with a NAP-5 column (GE Healthcare, Piscataway, NJ) equilibrated in 50 mM phosphate buffer with 150mM NaCl, pH 7.4 according to the manufacture's manual. Elution was ethanol precipitated, reconstituted in distilled water, and stored in -20 °C for future conjugation step.

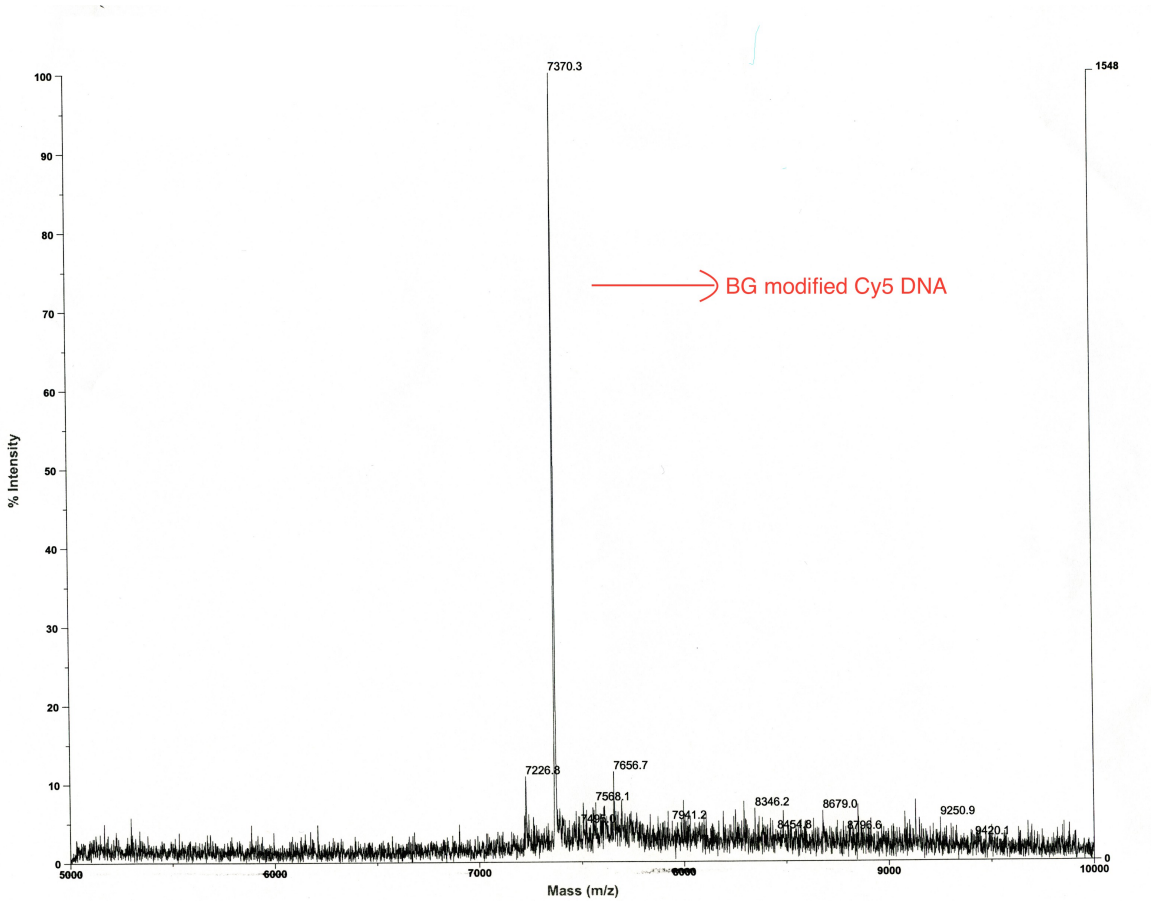

Figure 2.9. MALDI-TOF mass spectrometry analysis of benzylgruanine (BG) modified Cy5 DNA. After conjugating BG with Cy5-DNA (Seq1), the product DNA (peak mass) has a mass shift of +370.

Preparation of Thiol-modifed DNA

The following DNA sequence was used (11, 12)

Sequence2: (seq2): 5'– TCA TAC GAC TCA CTC TAG GG – 3'

DNA oligonucleotides with seq2 modifications were purchased from Integrated DNA Technologies (Coralville, IA). Thiolated DNA seq2 was modified with a C6 Thiol Modifier on the 5' end of the strand. DNA oligonucleotides were dissolved in TE buffer to a concentration of 5 mg/ml and precipitated in ethanol. Ethanol precipitated DNA were re-hydrated and stored in distilled water. For supported lipid bilayer experiments, thiolated DNA SH.seq2 was reduced by tris (2-carboxyethyl) phosphine (TCEP) buffer for 90 minutes at 37 °C before using for

bilayer experiments. TCEP buffer was prepared with 0.5 mM TCEP (pH 8), 10 mM 4-(2-hydroxyethyl)-1-piperazineethanesulfonic acid buffer (HEPES, pH 8). After 90 minutes of incubation, DNA was filtered through two Bio-spin 6 columns (Biorad, Hercules, CA) that were equilibrated in 50 mM phosphate buffer with 150 mM NaCl, pH 7.4, and then DNA was ready for bilayer experiments.

Preparation of RGD-Alexa488-DNA

Cyclic RGD peptide (cyclo (Arg-Gly-Asp-D-Phe-Lys)) was obtained from Pepnet, KY. RGD peptide was dissolved in 100 mM HEPES buffer to a concentration of 10 mM. SM (PEG) 2 (PEGylated SMCC crosslinker) (Life technologies, Grand Island, NY) consisting NHS ester and maleimide reactive groups were used to react with Lys-RGD and later with thoil modified DNA oligonucleotides (described below). 4 molar mass equivalents of SM (PEG) 2 (PEGylated SMCC crosslinker) were added to Lys-RGD solution in 100 mM HEPES buffer, and incubated at room temperature for an hour or longer until reaction was completed. Completion of the reaction was analysed by MALDI mass spectrometry to obtain a final product of RGD-maleimide. The reaction was purified by reverse phase C18 column HPLC, and fractions were analysed by MALDI mass spectrometry (Figure 2.10.a.).

DNA oligonucleotides (seq 2) with a C6 thiol modifier on the 5' end of the strand and a C6 amino modifier on the 3' end of the strand was synthesised and purified by Integrated DNA Technologies (Coralville, IA). DNA oligonucleotides were dissolved in TE buffer to a concentration of 5 mg/ml and precipitated in ethanol. To label DNA with a fluorescent probe, Alexa Fluor® 488 5-TFP (Alexa Fluor® 488 Carboxylic Acid, 2,3,5,6-Tetrafluorophenyl Ester), 5-isomer (Life technologies, Grand Island, NY) was used. Alexa 488 probe was used with 10 molar equivalents of DNA, 50 mM bicarbonate in 50 mM phosphate buffer with 150 mM NaCl, pH 7.4 buffer was added in the reaction. The reaction was incubated at room temperature for 2 hours, and then MALDI mass spectrometry confirmed the completion of the reaction (Figure 2.10.b.). Product of Alexa488-DNA was then desalted in NAP5 column, ethanol precipitated, and rehydrated in distilled water, and kept in -20 °C for storage as previously described.

To further conjugate thiol-Alexa488-DNA with RGD-maleimide, DNA was reduced with TCEP and desalted with Bio-spin6 columns (Biorad, Hercules, CA) as previously described. Reduced thiol-Alexa488-DNA then reacted with 2 molar equivalents of RGD-maleimide for 2 hours at room temperature followed by MALDI mass spectrometry (Figure 2.10.c.). A peak of mass change was detected to indicate the reaction completion. The reaction was purified by reverse phase C18 column HPLC, and fractions were analysed by MALDI mass spectrometry.

Purified RGD-Alexa488-DNA was ethanol precipitated, reconstituted in distilled water, and stored at -20 °C.

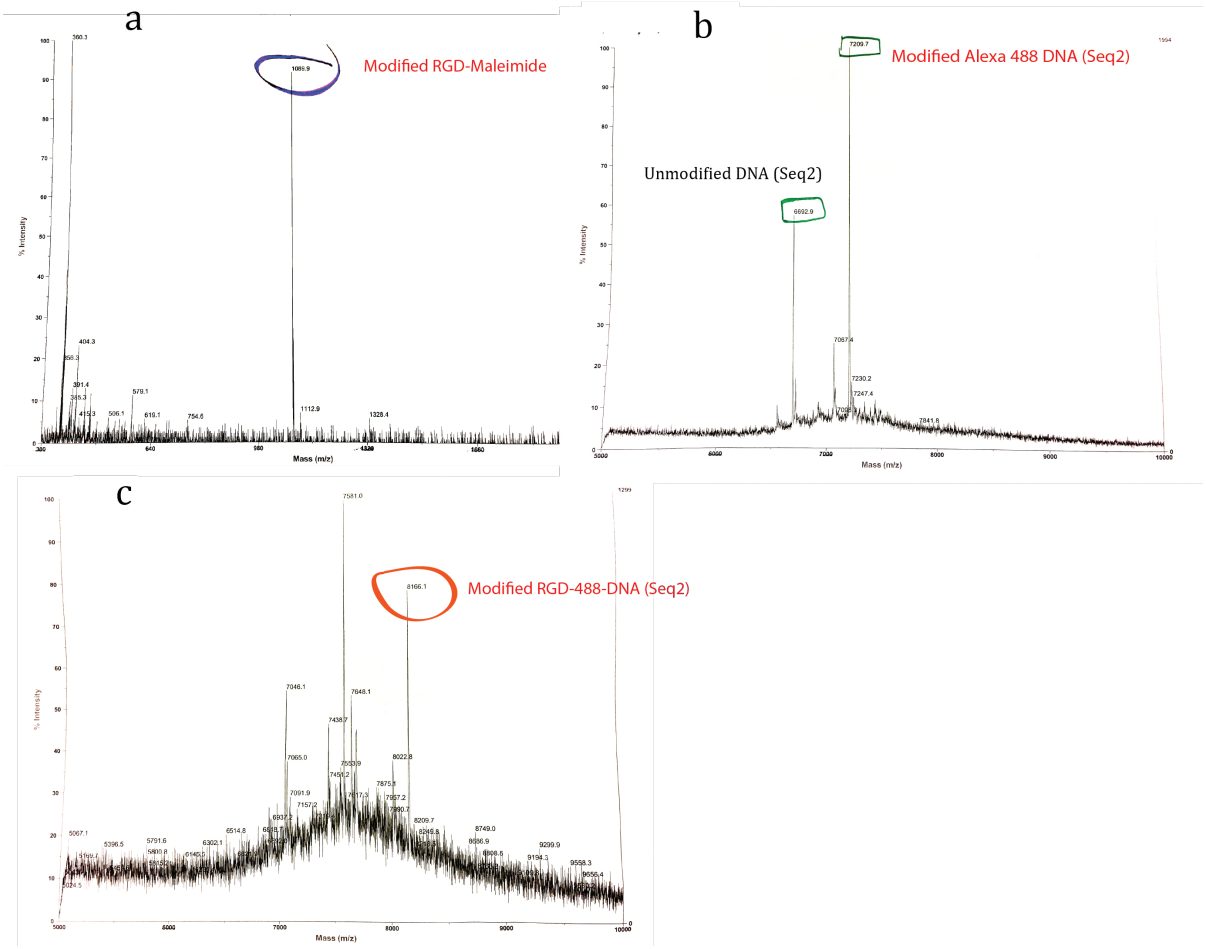

Figure 2.10. MALDI-TOF mass spectrometry analysis of RGD-Alexa488-DNA synthesis. a. MALDI-TOF analysis of modified RGD peptide with Maleimide linker to obtain RGD-Maleimide with +487 mass shift. b. MALDI-TOF analysis of modifying thoil-DNA (seq2) to obtain Alexa488-DNA(seq2) with +515 mass shift. c. MALDI-TOF analysis of conjugating RGD-Maleimide with thoil-DNA(seq2) to obtain RGD-488-DNA with +957 mass shift.

Synthesis of Benzylguanine DNA and ephrinB2-SNAP-tag His10

Benzylguanine(BG)-Cy5 DNA oligonucleotides with sequence1 were prepared as previously described. BG-Cy5 DNA were added to 2 molar equivalents of ephrinB2-SNAP-tag-His10 protein, after which the reaction was left at 37 °C for 60 minutes. The reaction was kept at 4 °C overnight before chromatography purification. The next day, the reaction was filtered through a 0.22 μm microcentrifuge spin filter at 5000 g for 5 minutes, and then purified with a Superdex 200 size exclusion chromatography column using AKTAexplorer system (GE healthcare, Buckinghamshire, United Kingdom). EphrinB2 SNAP-tag Cy5-DNA conjugate was separated and purified from free DNA and free dyes (Figure 2.11.). The product was then analysed using sodium dodecyl sulfate polyacrylamide gel electrophoresis (SDS-PAGE) to confirm the molecular weight of the conjugate (Figure 2.11.)

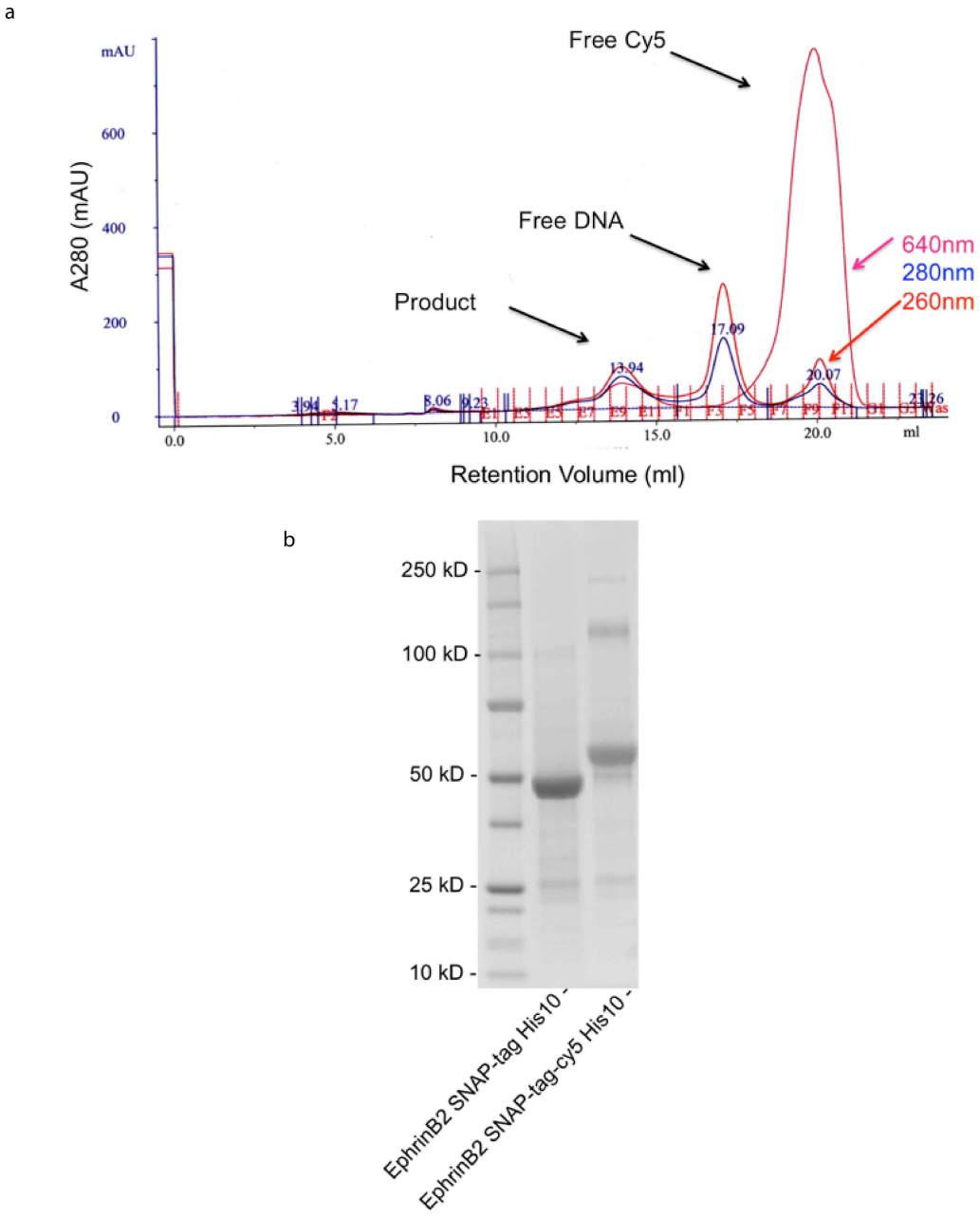

Figure 2.11. Purification of benzylguanine (BG) and Cy5 modified DNA to ephrinB2-SNAP tag His10 fusion protein. a. The product was purified by size exclusion chromatography to separate free DNA and free Cy5 fluorescent dye in the reaction. b. The results of the reaction were analysed by SDS-PAGE gel electrophoresis followed by Sypro Ruby stain. Black bands indicated molecular weight of the ephrinB2-SNAP tag His10 fusion protein before and after reacting with BG-Cy5-DNA.

Preparation of the supported lipid bilayer

Fisher brand circular or square microscope cover glasses with 1.5 thicknesses were used. Coverslips were soaked in 1:1 (vol/vol) 2-propanol and distilled water overnight, and were sonicated for 30 minutes the next day. Coverslips were rinsed thoroughly with distilled water and then etched in piranha solution 1 : 3 (vol/vol) mixture of hydrogen peroxide and sulfuric acid for 20 minutes. Rinsed coverslips were dried using a nitrogen stream. Lipids were purchased through Avanti Lipids (Alabaster, AL). Standard methods were employed to produce lipid vesicles (2). DOPC (1,2-dioleoyl-*sn*-glycero-3-phosphocholine) and 1,2-dioleoyl-sn-glycero-3-phosphoethanolamine-*N*-[4-(*p*-maleimidomethyl) cyclohexane-carboxamide] (MCC-DOPE) were mixed in a chloroform solution followed by evaporating with a rotary evaporator. The lipids were further dehydrated under a nitrogen stream for 30-60 minutes. Lipid vesicles were rehydrated in distilled water to a final concentration of 0.5 mg/ml. The hydrated lipid vesicles were then sonicated for 1 minute to generate a small unilamellar liposome vesicle (SUV). SUV was diluted with 1x phosphate buffered saline (PBS) and the mixture of SUV in PBS was deposited and incubated on a Piranha etched dry coverslip for 30 minutes to allow the formation of a supported lipid bilayer. After 30 minutes of incubation, the bilayer was rinsed in an excess of PBS buffer.

Functionalised DNA and protein on bilayer

2 mg/ml Casein in 1x PBS buffer was added to bilayer for 10 minutes to block unspecific binding then washed by PBS. DNA SH.seq2 was reduced with reducing agent TCEP for 90 minutes in 37 °C and desalted with Bio-spin 6 columns as previously described. Reduced DNA then was added to the pre-formed supported lipid bilayer containing 5% Maleimide lipid MCC-DOPE and 95% DOPC lipid and incubated for 90 minutes. Bilayer was washed with 1x PBS buffer after 90 minutes incubation. Final solution concentration of 100 nM Cy5-DNA-ephrinB2-SNAP-tag protein was added to the bilayer and incubated for 1 hour. Bilayer was washed with PBS after protein incubation.

Optical microscopy

FRAP, RICM, epifluorescent, and bright field images were taken on a motorized inverted microscope (Nikon Eclipse Ti-E/B, Technical Instruments, Burlingame, CA) using a Nikon 100x Apo TIRF 1.49 NA oil immersion objective. The microscope was equipped with a mortorised Epi/TIRF illuminator, a motorized Intensilight mercury lamp, a Nikon Perfect Focus system (Technical Instruments, Burlingame, CA), a motorised stage (ASI MS-2000, Eugene, OR), and an Orca-R2 interline charge-coupled device camera (Hamamatsu, Hamamatsu, Japan). Dichroics were 2 mm thick and mounted in metal cubes to preserve optical flatness: ZT488rdc, ZT561rdc, and ZT640rdc. Three different long-pass emission filters were used: ET500lp, ET575lp, and ET660lp. Bandpass emission filters were installed below the dichroic turret in a motorised filter wheel (Sutter Lambda 10-3, Novato CA): ET525/50m, ET600/50m, and ET700/75m. RICM was performed using a 50/50 beam splitter with a D546/10 filter. 100 mW 561 nm optically pumped solid state laser (Coherent Sapphire, Santa Clara CA), and 100 mW 640 nm diode laser (Coherent Cube, Santa Clara CA) were used for TIRF experiments. All FRAP, TIRF, epifluorescent filters and dichroics were purchased from Chroma (Bellows Falls, VT).

For confocal microscopy, we used the following lasers: 200mW 488 Ar-ion laser (Spectra Physics 177G, Santa Clara, CA), 100 mW 561 nm optically pumped solid state laser (Coherent Sapphire, Santa Clara CA), and 100 mW 640 nm diode laser (Coherent Cube, Santa Clara CA). All lasers were operated using an acousto-optic tunable filter and aligned into a dual-fiber launch built by Solamere (Salt Lake City, UT). One single-mode polarisation maintaining fiber (Oz Optics, Ottawa, Canada) was connected to a TIRF illuminator, whereas the other was connected to the spinning disk confocal unit. A spinning disk confocal head was custom fit to the microscope and camera (Yokogawa CSU-X1-M1N-E, Solamere, UT). The dichroic in the spinning disk head was a T405/488/568/647 multiline (Semrock, Rochester, NY). Emission filters were purchased from Chroma (Bellows Falls, VT) and in a custom-mounted filter wheel (ASI FW-1000): ET525/50M, ET605/52M, and ET700/75M. Confocal images were captured using a 1024 by 1024 pixel electron-multiplying charge-coupled device camera (Andor iXon3 888, Belfast, Ireland), typically at gain setting 200 and with pixels binned 1x1. Axial slice step size was 0.5 mm and extended 20 mm above the coverslip.

Live-cell imaging was performed using a stage-top incubator and objective heater (Chamlide TC-A, Quorum Technology, Guelph, Canada).

Fluorescence correlation spectroscopy (FCS)

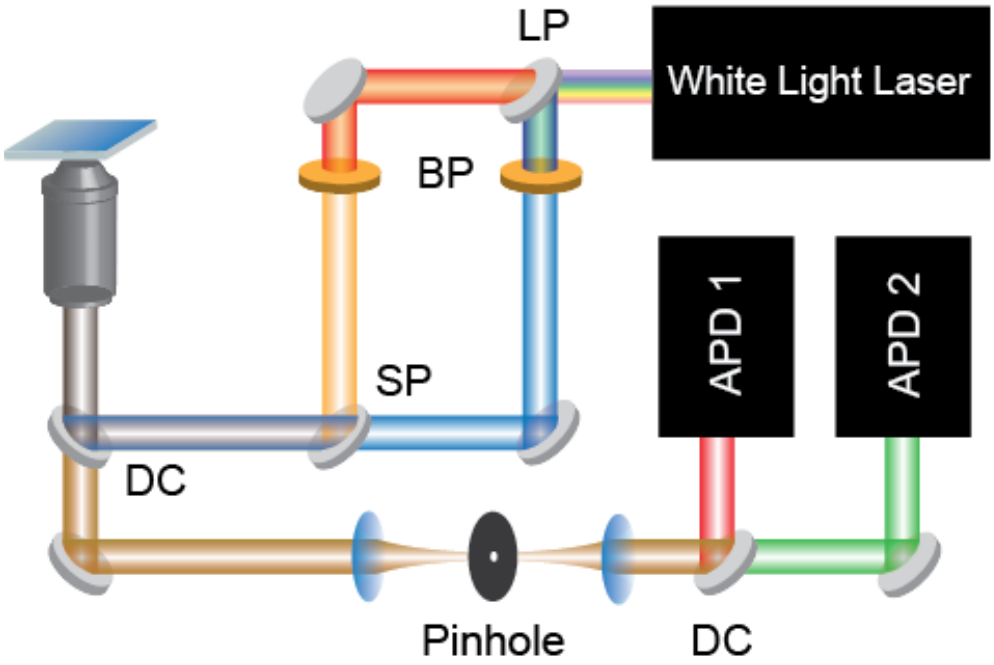

Figure 2.12. Setup for dual-colour FCS. Wavelengths from the white light laser are selected with a longpass filter (LP) and bandpass filters (BP). They are combined by a shortpass dichroic (SP) and sent to the inverted microscope via an optical fiber (not shown) in the epifluorescence geometry. Fluorescence signal collected by the 100x objective, and spatially filtered by the confocal pinhole. Two color signals are split by dichroic (DC) and recorded by avalanche photodiode detectors (APDs).

Dual-colour FCS (Figure 2.12.) was performed on a home-built spectrometer with a modified inverted microscope (Nikon TE2000). For excitations of fluorescent molecules, wavelengths selected by bandpass filters from a pulsed white light laser source (SuperK Extreme EXW-12, NKT Photonics) were used. The excitation pulses are sent into a single mode optical fiber, after which the combined pulses enter the microscope through a multi-color dichroic cube (Di01-R405/488/561/635-25x36, Semrock). Notch filters were used to remove excess excitation intensity. The fluorescence signal was collected by the 100x high-NA oil immersion objective and recorded by avalanche photodiode detectors (Hamamatsu). The signal is directly converted into autocorrelation signal by a hardware correlator (Correlator.com). In the FCS experiments

described in the main text, blue light (488 nm) was used to excite Alexa Fluor 488, and red light (640 nm) for exciting Cy5 simultaneously. The average power used to excite the sample ranged between 0.5 and 5.0 μW, depending on the fluorophore quantum yield and the surface density, which is equivalent to the irradiance range of 0.4 $\sim$ 4.0 kW/cm^2 calculated with the calibrated spot sizes. The resulting autocorrelation $G_0(\tau)$ was fit to the two-dimensional Gaussian diffusion model (20),

$$\mathrm{G_0(\tau)} = \frac{1}{N}\left(\frac{1}{1+\tau/\tau_D}\right)$$

Here τ is time delay, N is the number of particles in the focus spot, and τ_D is the diffusion correlation time. To calibrate the spot size of the confocal focus, N of a bilayer with a known surface density of fluorescent lipids of each color, BODIPY-FL-DHPE and ATTO665-DPPE for 488 nm 640 nm were measured, which consistently yielded the radius of 0.20 ± 0.01 μm and 0.27 ± 0.01 μm for 640 nm, respectively. The diffusion coefficient D was calculated by using the relation

$$D = w^2/4\tau_D$$

Here w is the radius of the focus spot size.

Some fluorescent molecules such as Cy5 exhibit fast blinking kinetics due to a long-lived triplet state that contributes to the photo-physics. In FCS, blinking appears on the microsecond to millisecond timescales. For these dyes, the autocorrelation model requires an extra term to the two-dimensional Gaussian diffusion model in order to account for the additional intensity fluctuation from blinking,

$$\mathrm{G(\tau)} = \left(\frac{1-F+Fe^{-\frac{\tau}{\tau_e}}}{1-F}\right)\mathrm{G_0(\tau)}$$

Here F is the fraction of molecules in the dark state at equilibrium, and τ_e is the lifetime of the dark triplet state.

Image analysis

Micromanager (UCSF, CA) and ImageJ software were used to collect, analyse, and process the images.

Neural stem cell culture

NSCs were isolated from the hippocampi of adult female Fischer 344 rats. NSCs used in this work were obtained from David Schaffer Lab (UC Berkeley, CA); passages 31-38 were cultured for experiments. NSCs were cultured on Polyornithine/Laminin coated plates for all non-supported lipid bilayer conditions. For NSCs maintenance and proliferation assay, NSCs were cultured in Dulbecco's Modified Eagle Medium: Nutrient Mix F-12 (DMEM/F-12) with HEPES and L-Glutamine (Invitrogen, CA) supplemented with 1% (v/v) N-2 supplement (Invitrogen, Carlsbad, CA), and 20 ng/ml recombinant human basic fibroblast growth factor (FGF-2)(Peprotech, NJ). Accutase (Innovative Cell Technologies, CA) was used for cell detachment.

Engineering EphB4 m-cherry cell line

An NSC line expressing an EphB4-mCherry fusion protein was generated. Rat EphB4 was isolated from cDNA derived from the NSCs and fused to a florescent protein mCherry, and cloned into the retroviral vector CLPIT (Schaffer lab, UC Berkeley). Retroviral vectors were packaged using standard protocol, as described in prior work (21). NSCs were infected at an MOI of 1, and cultures were selected using puromycin at a concentration of 0.6 μg/mL to create a stable cell line.

Antibody blocking experiment

For testing NSC attachment on supported membrane and Eph-ephrin binding specificity, goat antibodies to EphB4 and EphB2 (Santa Cruz Biotechnology, Dallas, Texas) were used. Cells were centrifuged and suspended in 1x PBS buffer, antibodies were incubated with cells for 1 hour at 4 °C before seeding on ephrinB2 bilayer.

Section 2.4: Chapter 2 references

1. Nye JA & Groves JT (2008) Kinetic Control of Histidine-Tagged Protein Surface Density on Supported Lipid Bilayers. *Langmuir : the ACS journal of surfaces and colloids* 24:4145-4149.
2. Lin W-C, Yu C-H, Triffo S, & Groves JT (2010) Supported Membrane Formation, Characterization, Functionalization, and Patterning for Application in Biological Science and Technology. *Current Protocols in Chemical Biology* 2(2):235-269.
3. Yoshimura Y & Fujimoto K (2008) Ultrafast Reversible Photo-Cross-Linking Reaction: Toward in Situ DNA Manipulation. *Organic Letters* 10(15):3227-3230.
4. Fujimoto K, Konishi-Hiratsuka K, Sakamoto T, & Yoshimura Y (2010) Site-Specific Cytosine to Uracil Transition by Using Reversible DNA Photo-crosslinking. *Chembiochem : a European journal of chemical biology* 11(12):1661-1664.
5. Peng X, Hong IS, Li H, Seidman MM, & Greenberg MM (2008) Interstrand Cross-Link Formation in Duplex and Triplex DNA by Modified Pyrimidines. *Journal of the American Chemical Society* 130(31):10299-10306.
6. Nagatsugi F & Imoto S (2011) Induced cross-linking reactions to target genes using modified oligonucleotides. *Organic & Biomolecular Chemistry* 9(8):2579-2585.
7. Chung M, Lowe RD, Chan YH, Ganesan PV, & Boxer SG (2009) DNA-tethered membranes formed by giant vesicle rupture. *Journal of structural biology* 168(1):190-199.
8. Chan YH, van Lengerich B, & Boxer SG (2009) Effects of linker sequences on vesicle fusion mediated by lipid-anchored DNA oligonucleotides. *Proceedings of the National Academy of Sciences of the United States of America* 106(4):979-984.
9. Rawle RJ, van Lengerich B, Chung M, Bendix PM, & Boxer SG (2011) Vesicle fusion observed by content transfer across a tethered lipid bilayer. *Biophysical journal* 101(8):L37-39.
10. Selden NS*, et al.* (2012) Chemically programmed cell adhesion with membrane-anchored oligonucleotides. *Journal of the American Chemical Society* 134(2):765-768.
11. Hsiao SC*, et al.* (2009) Direct cell surface modification with DNA for the capture of primary cells and the investigation of myotube formation on defined patterns. *Langmuir : the ACS journal of surfaces and colloids* 25(12):6985-6991.
12. Coyle MP, Xu Q, Chiang S, Francis MB, & Groves JT (2013) DNA-Mediated Assembly of Protein Heterodimers on Membrane Surfaces. *Journal of the American Chemical Society* 135:5012-5016.

13. Keppler A*, et al.* (2003) A general method for the covalent labeling of fusion proteins with small molecules in vivo. *Nature biotechnology* 21(1):86-89.
14. Engin S*, et al.* (2010) Benzylguanine thiol self-assembled monolayers for the immobilization of SNAP-tag proteins on microcontact-printed surface structures. *Langmuir : the ACS journal of surfaces and colloids* 26(9):6097-6101.
15. Moran U, Phillips R, & Milo R (2010) SnapShot: key numbers in biology. *Cell* 141(7):1262-1262 e1261.
16. Knight JD, Lerner MG, Marcano-Velazquez JG, Pastor RW, & Falke JJ (2010) Single molecule diffusion of membrane-bound proteins: window into lipid contacts and bilayer dynamics. *Biophysical journal* 99(9):2879-2887.
17. Diehl S*, et al.* (2005) Altered expression patterns of EphrinB2 and EphB2 in human umbilical vessels and congenital venous malformations. *Pediatric research* 57(4):537-544.
18. Ashton RS*, et al.* (2012) Astrocytes regulate adult hippocampal neurogenesis through ephrin-B signaling. *Nature neuroscience* 15(10):1399-1406.
19. Salaita K*, et al.* (2010) Restriction of receptor movement alters cellular response: physical force sensing by EphA2. *Science* 327(5971):1380-1385.
20. Bacia K, Haustein E, & Schwille P (2014) Fluorescence correlation spectroscopy: principles and applications. *Cold Spring Harbor protocols* 2014(7):709-725.
21. Lim K-i, Klimczak R, Yu JH, & Schaffer DV (2010) Specific insertions of zinc finger domains into Gag-Pol yield engineered retroviral vectors with selective integration properties. *Proceedings of the National Academy of Sciences* 107(28):12475-12480.

Chapter 3

Section 3.1: NSCs differentiation on an ephrinB2 supported lipid bilayer

Isolated *in vitro* NSCs carry the unique capacity for self-renewal and differentiation into three lineage specific cell types: neurons, astrocyte, and oligodendrocytes (1, 2). Previous studies have demonstrated that ephrinB2 signalling can promote neuronal differentiation in NSCs using antibodies that pre-cluster ephrinB2 ligands in solution (3). However, the solution studies cannot reflect the geometry and biophysical properties of Eph receptor signalling because both Eph receptors and ephrin ligands are membrane bound, and so their signalling activation is contact dependent. Another disadvantage from antibody-cluster based solution studies is that it is very challenging to precisely control the size or the oligomer state of receptor-ligand complexes. A recent follow-up study also demonstrated the role of multivanlency of ephrinB2 clusters in regulating neuronal differentiation. In this work, the authors generated a synthetic multivalent ligand complex by conjugating ephrinB2 ligands with a chain of high molecular weight biopolymer hyaluronic acid (HA), by using this method 2-25 ephrinB2 molecules per HA chain (4) can be generated. Both studies demonstrated that multivalency of ephrinB2 ligands regulated NSCs behaviours, and suggested that higher cluster size and concentrations of ephrinB2 ligands promote neuronal differentiation. DNA origami nanocalipers have also been used to spatially control EphA receptor functions in MDA-MB-231 cancer cells (5). Nevertheless, studies using membrane-bound monomeric ephrinB2 to activate NSCs signalling have yet to be explored.

A hybrid system coupling live cells to a supported lipid bilayer for the purposes of studying EphB4-ephrinB2 signalling in NSCs was described in Chapter 2. We were able to successfully functionalise ephrinB2 ligands on a fluid supported membrane through a DNA-SNAP-tag based approach. EphrinB2 ligands were anchored to lipid molecules, which consequently inherited the mobility characteristics of lipid bilayer. This setup recapitulates the chemical composition and the physical geometry of membrane associated receptor-ligand signalling and provides a more realistic physiological microenvironment for studying membrane receptor signalling in cell-cell communication. In Chapter 2, we also confirmed the binding specificity between membrane bound ephrinB2

ligands and EphB4 receptors on NSCs surface by TIRF and confocal microscopies. To continue the investigations of the effect of EphB4-ephrinB2 signalling on NSCs functions, differentiation experiments of NSCs were performed on an ephrinB2-displaying supported lipid membrane.

NSCs were cultured on ephrinB2 displaying supported membrane for 5 days of differentiation studies. For this condition, ephrinB2 ligands provided the only physical linkage between the lipid bilayer and the apposing NSCs. In Chapter 2, we developed the DNA-SNAP-tag based conjugation method to tether ephrinB2 ligands onto lipid bilayer. This biochemical conjugation permits ephrinB2 ligands to be stable and efficient for NSCs differentiation studies. Previous results have shown that NSCs were able to adhere to the supported membrane from the exclusive binding and clustering with ephrinB2 ligands. To assure that NSCs can reside and form adhesion on lipid bilayer for a 5-day differentiation process, we added adhesion molecule Laminin protein to the cell culture medium 12 hours after cells were seeded on the ephrinB2 bilayer. The reason for doing this is that prior experiments have shown that bilayers and proteins are likely to degrade after 12 hours. Indeed, we have observed NSCs detach from defected bilayers after 12 hours (data not shown). In the presence of Laminin protein, cells were able to stably adhere onto a bilayer underlying glass substrate over a course of 5 days. For this culture condition, NCSs were exposed and engaged to ephrinB2 ligands for a relatively short time scale; Laminin protein was added into bilayer culture 12 hours later.

We included five other culture conditions in this study to compare with the differentiation outcomes triggered by ephrinB2-EphB4 signallings. For the first two additional culture conditions, we cultured NSCs with medium consisting antibody pre-clustered soluble ephrinB2 ligands on Laminin coated glass at day 1 only and day1-5 respectively. It was previously demonstrated that multivalent ephrinB2 clusters in solution regulate neuronal differentiation of NSCs (3, 4). For the third and fourth additional culture conditions, a positive control condition of conventional soluble factor induced differentiation on Laminin coated glass was included, as well as a negative control condition in which cells were cultured in survival medium. Additional bilayer condition (fifth additional condition) was studied to directly compare with the ephrinB2 bilayer differentiation results. NSCs were treated with anti-EphB4 antibodies that specifically block the ligand binding sites of EphB4 receptors before seeding on ephrinB2 bilayer. The results from this experiment will be valuable, and will establish whether inhibition of ephrinB2-EphB4 signalling affects NSCs function.

After 5 days of neural stem cell in culture under mixed conditions, cells were fixed and immunostained with neuronal lineage marker βIII-tubulin and nuclei marker 4',6-diamidino-2-phenylindole (DAPI). We recorded the

fluorescent intensities of neuronal marker on every cell, and set up an intensity threshold to select for βIII-tubulin positive cells. DAPI staining presented the total number of cells in each condition, and we calculated the ratio of number of positively stained βIII-tubulin cells over the number of DAPI stained cells. Figure 3.1.a illustrates the differentiation results across six conditions. The ephrinB2 bilayer culture condition yielded a 36.6% population of βIII-tubulin positive cells, indicating neuron lineage distribution. This result showed roughly equal proportions of neuronal differentiation (35.6%) to positive control condition: retinoic acid (RA) and fetal bovine serum (FBS) containing culture on Laminin coated glass. RA and FBS are known soluble factors that induce neuronal differentiation. Equal proportions of neuronal differentiation between ephrinB2 bilayer culture and RA/FBS soluble culture indicated the functional role of EphB4-ephrinB2 signalling in promoting neural stem cell function. However when NSCs were pre-blocked with antibody against ephrinB2 binding sites on EphB4 receptors, we saw an inhibitory effect on neuronal differentiation (20.3% positive βIII-tubulin population). This inhibitory effect strongly suggested that neuronal differentiation triggered in ephrinB2 bilayer was controlled by EphB4 receptor signalling. The proportions of neurons generated from soluble Fc-ephrinB2 conditions were generally lower and less efficient. For soluble Fc-ephrinB2 experiments, when pre-clustered Fc-ephrinB2 ligands were supplied only at the beginning of Day 1 culture, 14% neurons were generated. This result is similar to survival culture condition (medium containing 0.1ng/ml of FGF-2) on Laminin coated glass, there was as low as 14% neurons differentiation. However, when soluble Fc-ephrinB2 was provided in the culture medium continuously throughout an entire course of 5 days, neuronal differentiation was promoted to a higher level of 28.6%. Nevertheless, the result is still lowered than ephrinB2 bilayer induced differentiation.

These data demonstrate the functional role of membrane bound monomeric ephrinB2 ligands in inducing neuronal differentiation when tethering to a supported membrane. Reconstituted signalling on a supported membrane reflects the realistic spatial organisation of Eph-ephrin signalling, allowing monomeric ephrinB2 ligands to diffuse laterally and cluster with EphB4 receptors. Both membrane bound monomeric ephrinB2 on supported membrane and pre-clustered Fc-ephrinB2 in solution have been shown to regulate NSCs lineage commitment in neuronal differentiation. We have found that the membrane bound monomeric ephrinB2 ligands signal much more efficiently than clustered soluble Fc-ephrinB2 ligands in NSCs differentiation. Signalling provided from membrane bound ephrinB2 ligands was valid only for the initial 12 hours, as bilayers and ligands degradation took place shortly after. For a similar time scale, 1 day supplements of soluble Fc-ephrinB2 clusters supplement were not sufficient to cause differentiation. They yielded equal proportions of neurons as negative control experiment (in survival culture). When soluble Fc-ephrinB2 was present

for the entire course of 5 days, it resulted similar neuronal differentiation to membrane bound monomeric ephrinB2 signalling which only present at hourly time scale.

Data from immunofluorescent staining also demonstrated different morphologies of neurons differentiated from different signalling conditions (Figure 3.1.b). Soluble differentiation factors FA and FBS induced neurons with morphologies of larger cell bodies, and with multiple and longer processes. Soluble Fc-ephrinB2 ligands induced neurons developed fewer processes. Membrane bound monomeric ephrinB2 signalling regulated neurons were able to generate multiple albeit shorter processes. These morphological differences suggested that each signalling condition may have different activation pathway for neural stem cell differentiation or have different strength in activating neuronal differentiation.

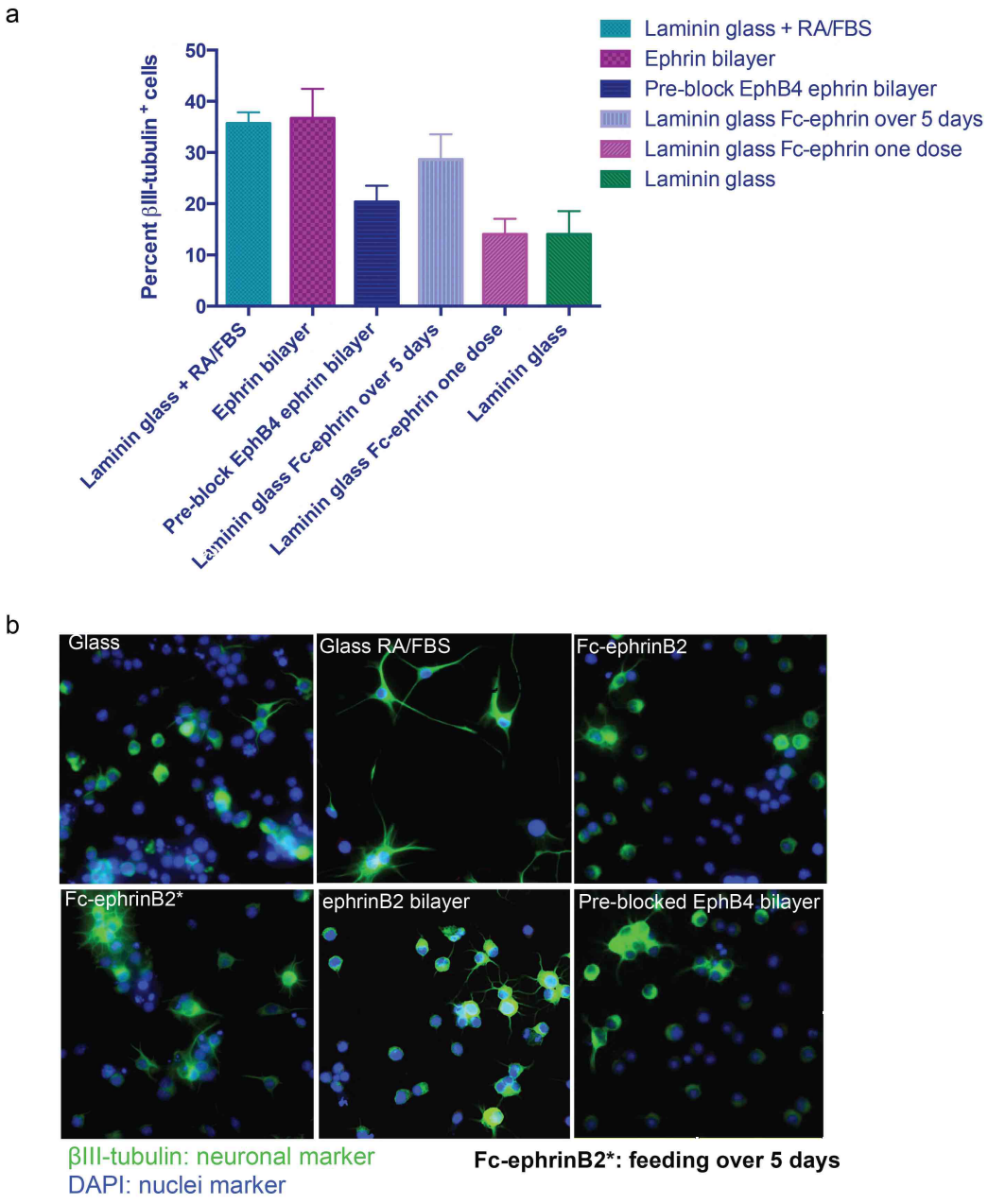

Figure 3.1. NSCs differentiation studies on ephrinB2 displayed supported membrane. a. βIII-tubulin positive cells. Error bars are mean ± standard error of mean, sample size n=3, more than 300 cells per sample was analysed. b. Epi-fluorescent images of immunostaining: neuronal marker βIII-tubulin (green) and DAPI (blue).

Section 3.2 Spatial mutation of EphB4 receptors alters neuronal differentiation in NSCs

A hybrid system of live cells on a supported membrane is suitable for studying the effect of spatial re-organisation on Eph-ephrin signalling (6-8) by applying a "spatial mutation" technique. By nanofabricating micro- or nano-structures, chromium (Cr) metal thin lines as narrow as 20 nm in width can be decorated on the glass solid support to generate lipid diffusion barriers. These Cr lines physically partition the supported lipid bilayer into separated lipid corrals. Ligands tethered onto the supported lipid membrane can only diffuse inside each lipid corrals since they cannot hop across the Cr diffusion barriers. In turn physical forces from Cr patterned diffusion barriers acting on ligands can alter receptor spatial organisation (6, 7, 9-11). Methods from photolithography and electron-beam lithography can be used to generate these micro corral structures (12-14).

Tyrosine kinase receptors such as Eph and their membrane bound ligands ephrin play a critical role in signal transduction since they reside where signalling initiates. These ligands and receptors bind and form higher order clusters to transduce signalling and activate downstream cellular events. Spatial regulation of cell surface receptors has been shown to modulate signal transduction pathway in cancer and development (15). In the NSCs niche, ephrinB2 ligands expressed on astrocyte cell surfaces signal with EphB4 receptors on NSCs to regulate neurogenesis, in particular promote neuronal differentiation (3, 4, 16). However the effect of spatial distribution in EphB4-ephrinB2 clusters in their signalling outcome has not been explored.

Spatial mutation has been successfully applied to investigate spatial organisation in immunological synapses (9-11, 13, 17) and more recently in EphA receptor signalling (6-8). In particular, EphA2 receptors have shown their sensitivity to the spatial and mechanical cues. By enforcing physical restrictions (diffusion barriers by spatial mutation) on receptor movement, downstream signalling and cellular outcome were altered (6-8). Since EphA receptors and EphB receptors belong to the same family of receptor tyrosine kinases, they share many seminaries in their crystal structures as well as physical properties such as ligand binding affinities, etc. (18-22). EphA and EphB receptors are also found to share common signalling pathways (23). Because of these structural and binding property assembly of EphA and EphB receptors, here we hypothesized EphB receptors are likely to be sensitive to the spatial mutation. When mechanical

ligand restriction extends to the spatial organisation of EphB4 receptor at cell surface junctions, in turn cellular response to ephrinB2 is altered. As a consequence, neuronal differentiation will be modulated by spatial mutation.

We physically manipulated EphB4 spatial organisation by employing spatial mutation. For implementation of spatial mutation, Cr substrates were nano-fabricated on glass coverslips by electron-beam lithography (procedure described in methods section). Supported membranes were formed on glass substrates with various fabricated patters of Cr lines typically 100 nm in width and 10 nm in height. These Cr lines served as diffusion barriers against lateral transport of EphB4 receptors. Lipid molecules and membrane tethered ephrinB2 ligands can diffuse freely but cannot cross the barriers, since their movements were restricted in each Cr line fabricated micro-corrals.

FRAP experiments have probed the diffusion properties of ephrinB2 ligands in corral membranes (Figure 3.2.). Images and fluorescent intensity line scan data showed that the corral-patterned membrane can be recovered after photobleaching. Molecules cannot cross the diffusion barrier into grid corral bilayer after bleaching. Upon binding to supported membrane tethered ephrinB2 ligands, the EphB4 receptors become subject to the geometrical restrictions to mobility.

Spatial mutation applies mechanical perturbations to the living NSCs exclusively through Eph-ephrin receptor-ligand couplings, and the entire ensemble of receptors is uniformly affected. EphB4 receptors were spatially re-organised by engaging NSCs with patterned membranes. After 40 minutes of neural stem cell landing on the supported membrane, fluorescent images of EphB4-ephrinB2 spatial re-distribution were taken (Figure 3.3.). EphB4 receptors movement and cluster formation were redistricted in 2 μm and 4 μm corrals. EphB4 receptors clustered and moved towards Cr lines, however cannot cross the lines. We also designed a control pattern with nano-fabricated Cr dots with 2 μm spacing. In this pattern, receptor-ligand movement is not restricted, because laterally diffusion of lipid molecules is not hindered.

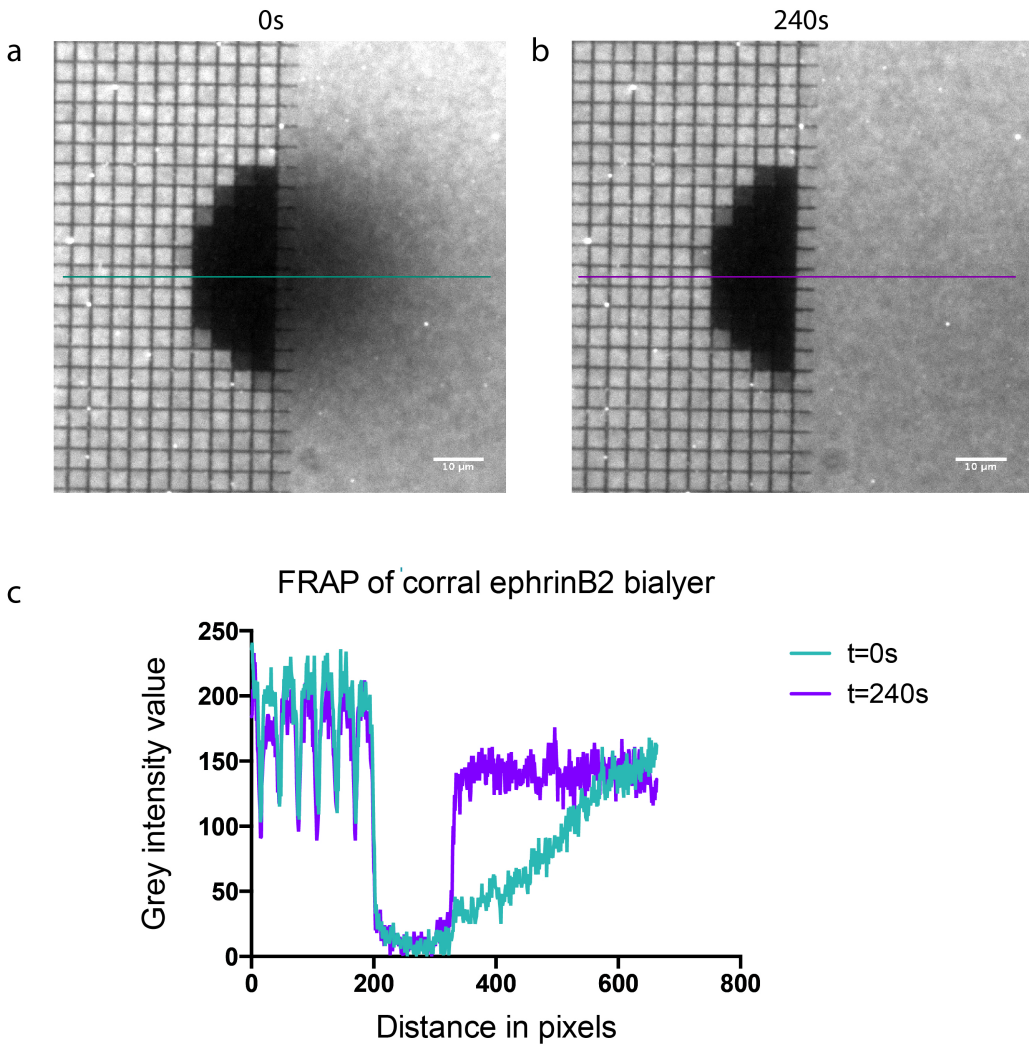

Figure 3.2. FRAP experiment from a nanofabricated 4 µm spacing Cr substrate underlying bilayer. a. A defined region on bilayer was photobleached with 647 nm epifluorescent light as shown at 0 second. b. After 240 seconds, a recovery image was taken. c. Line-scan intensity measurements were taken across the bleached area. Only the non-gridded areas were able to fully recover after photobleaching.

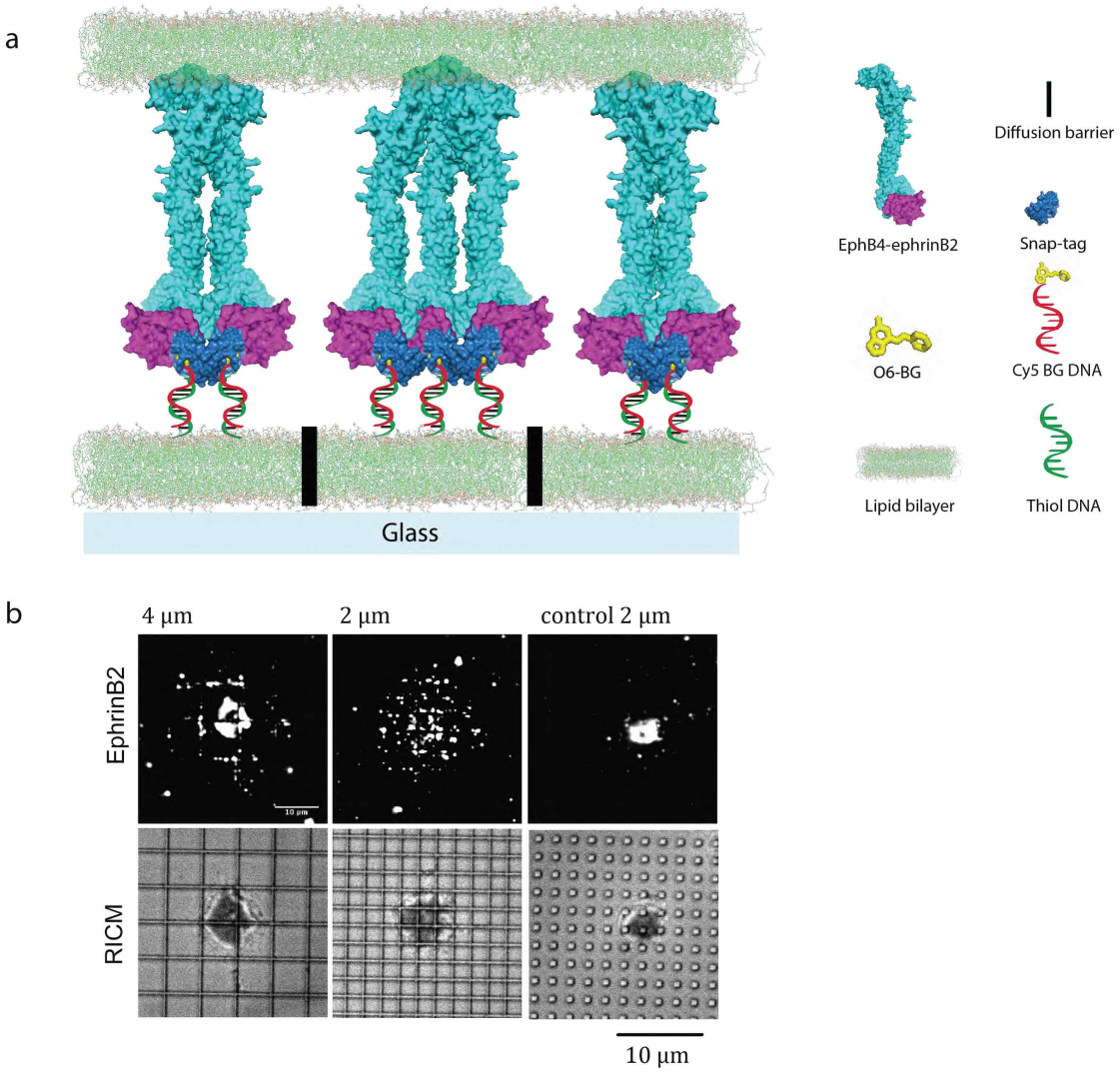

Figure 3.3. Schematic of spatial mutations: a A NSC expressing EphB4 interacting with a supported membrane displaying ephrinB2. a. Cr diffusion barriers physically perturb EphB4 receptor movement and cluster formation. b. TIRF and RICM images of ephrinB2 at the interface between neural stem cells and supported membrane on the 2, 4 μm and 2 μm control gridded substrates.

Using the technique of spatial mutation, we tested whether NSCs differentiation is affected by the mechanical properties of the membrane-cell interface. Specifically, we physically hindered EphB4-ephrinB2 re-organisation in NSCs with patterned supported membranes containing ephrinB2 ligands. We cultured NSCs on patterned supported membranes containing ephrinB2 ligands for 5 days. Cells were then fixed and immunostained with neuronal lineage marker βIII-tubulin, and we analysed the fluorescent intensities and quantified the population of βIII-tubulin positive cells (see Methods). Non-patterned, 5 μm, 3 μm, and control 2 μm patterned ephrinB2 bilayers were studies for differentiation assays.

The number of neurons generated on corral substrates with 5 μm, 3 μm, and control 2 μm revealed a significant decrease in the amount of neuronal differentiation on 3 μm grid size (Figure 3.4.). The non-patterned EphrinB2 bilayer without spatial mutation generated 24.5% neurons, 5 μm ephrinB2 bilayer generated 29%, and control 2 μm ephrinB2 bilayer had around 22.5% neuronal differentiation. While on 3 μm ephrinB2, there was a significant drop on neuronal differentiation, only 11.5% of βIII-tubulin positive cells were detected. There were same amount of ephrinB2 ligands tethered on all bilayer conditions from Day 1 culture. EphrinB2 ligand densities for all bilayer conditions were measured before seeding NSCs on supported membrane for differentiation experiments. Cells encountered approximately the same amount of ephrinB2 ligands across all spatial mutations. Inhibition of neuronal differentiation from 3 μm indicated that introducing a spatial and mechanical disruption of EphB4-ephrinB2 movement regulates NSCs function in neuronal differentiation. In parallel, under non-bilayer conditions, neuronal differentiation was observed at 27.3% and 15% for positive control RA/FBS and survival condition (negative control).

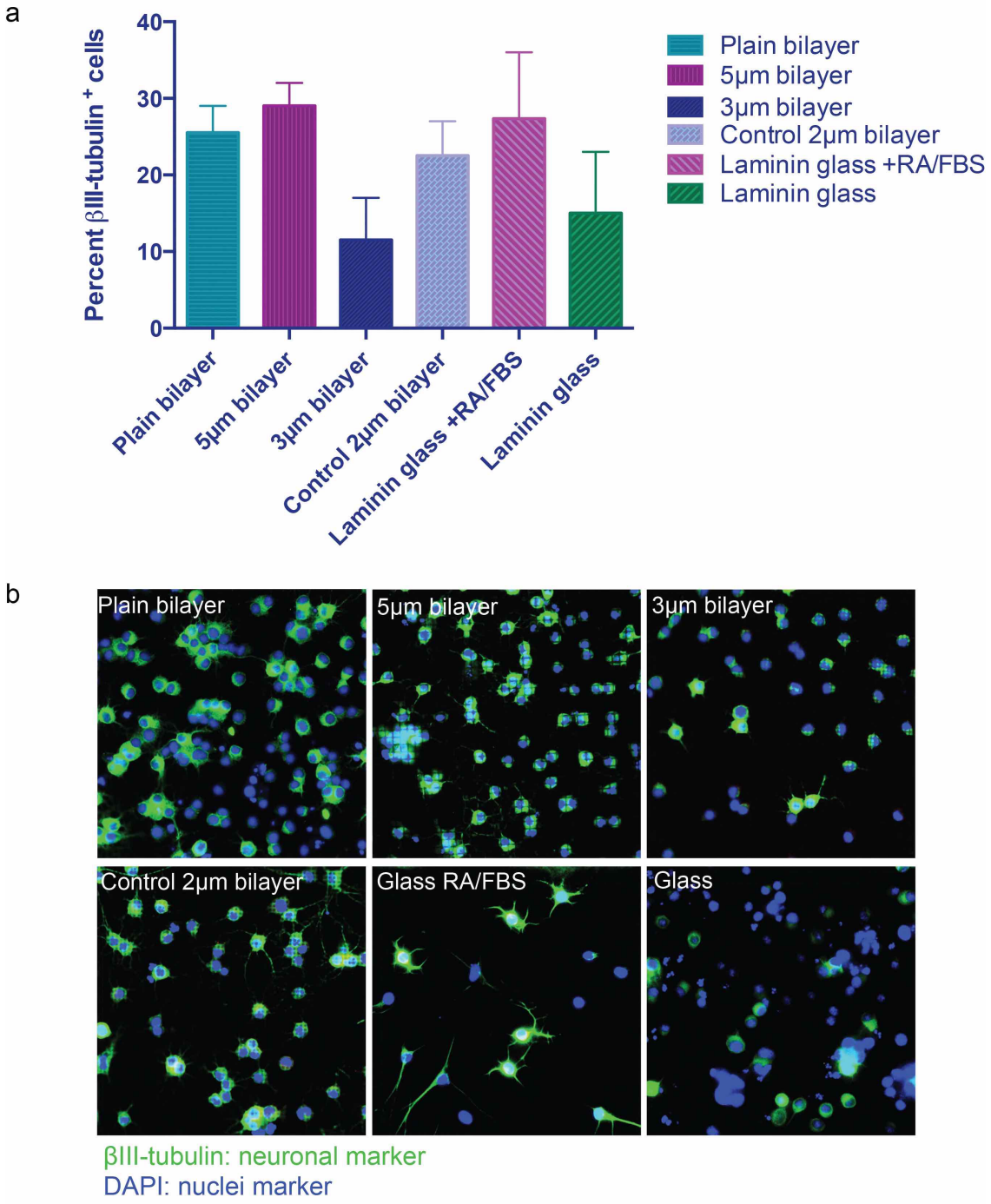

Figure 3.4. Spatio-mechanical regulation of EphB4-ephrinB2 signalling inhibits neuronal differentiation in NSCs. a. Results of differentiation study on ephrinB2 corral bilayers: populations of immunostained βIII-tubulin positive cells. Error bars are mean ± standard error of mean, sample size n=3, 300-1000 cells per sample were analysed. b. Epi-fluorescent images of fixed cells after 5 days: neuronal marker βIII-tubulin (green) and DAPI (blue).

Section 3.3: Materials and Methods

Preparation of supported lipid bilayer

Supported bilayers were prepared according to the procedures described in Chapter 2. DOPC and MCC-DOPE lipids were mixed in chloroform solution in a 20: 1 molar ratio. Lipid mixture was evaporated with a rotary evaporator for 30 minutes. Dried lipid film were hydrated in distilled water and sonicated to generate SUVs. SUVs were mixed with 1x PBS buffer to a final concentration of 0.25 mg/ml, and used immediately to form bilayers on piranha etched coverslips.

Functionalised DNA and protein on bilayer

A Maleimide incorporated (MCC-DOPC) bilayer was formed as previously described. The bilayer was blocked with 2mg/ml Casein in 1x PBS 10 minutes before thoil-DNA incubation. Thoil-DNA (DNA SH.seq2) was reduced in TCEP, desalted, then added to bilayer and incubated for 90 minutes. EphrinB2 ligands (Cy5-DNA-ephrinB2-SNAP) were added to bilayer and incubated for 1 hour. Bilayers were rinsed with 1xPBS buffer after protein incubation. Before seeding NSCs, bilayers were buffer exchanged with cell culture medium.

Neural stem cell culture and differentiation

NSCs were cultured in DMEM:F12+N2 media for proliferation as previously described in chapter 2. For differentiation studies, 8-well glass chamber slides were seeded with 2×10^4 cells per well. For negative control differentiation condition, NSCs were cultured in standard culture medium containing survival condition 0.5 ng/ mL FGF-2 (PeproTech, Rocky Hill, NJ). For positive control differentiation condition, NSCs were cultured in standard culture medium in the addition of 1 μM retinoic acid and 2 vol/vol% fetal bovine serum. Media changes were performed every 2 days.

For ephrinB2 bilayer differentiation studies, 0.5 ng/ mL FGF-2 was added to the medium for 5 days. Goat anti-mouse EphB4 antibody (R&D System, Minneapolis, MN) was used to block the EphB4 receptor ligand binding sites at 4 μg/ml for 30 minutes at 37 °C before seeding on ephrinB2 bilayer. 10 μg/ml of Laminin protein was added to all bilayer cell culture media 12 hours after at day 1. Media changes were performed every 2 days.

Antibody-clustered Fc-ephrinB2 formation

To generate soluble clustered ephrin-B2 complexes, recombinant mouse ephrinB2/Fc chimera (R&D Systems, Minneapolis, MN) was incubated with goat antibody to human IgG Fc-fragment specific (Jackson ImmunoResearch, West Grove, PA) at a 9:1 ratio (w/w) for 90 minutes at 4 °C before immediate use.

Nanofabrication

Fabrication of Cr grid substrates using photolithography

Cr grid substrates were patterned on a glass substrate using photolithography and subsequent Cr etching. For patterning, glass substrates were cleaned by sonication in acetone for 5 minutes. After sonication, substrates were rinsed with distilled water and dried with a stream of nitrogen. A 7-nm-thick Cr layer was deposited using e-beam evaporation at $5x10^{-6}$ torr. The deposition rate was maintained at ~0.01 nm s^{-1}. The Cr substrates were cleaned again by sonication in acetone for 5 minutes and rinsed with distilled water. Next, the substrates were dried by a stream of nitrogen and heated at 130 °C for 10 minutes to remove residual moisture. S1805 positive photoresist (PR) was spun on the pre-cleaned glass substrate at 4000 rpm for 35 second. The PR film-coated substrate was soft baked at 115 °C for 60 seconds. PR was exposed to UV through Quartz Cr mask with a UV dose of 27 mJ/cm^2. PR was developed in MIF-321 developer. To generate Cr patterns, the underlying Cr layer was etched through patterned photoresist mask using CR-7 Cr etchant (Cyantek Corporation, Fremont, CA). Finally, residual PR was removed using Microposit Remover 1165.

Fabrication of Cr grid substrates using e-beam lithography

Glass coverslips were bath-sonicated in distilled water for 5 minutes to remove gross particulate matter and followed by etching in piranha solution (3:1 ratio of H_2SO_4 : H_2O_2) for 5 minutes. Etched coverslips were rinsed with distilled water, immersed in isopropanol, and dried under a stream of nitrogen. Surface moisture was removed by heating at 140 °C for 10 minutes. Afterwards, coverslips were spin-coated for 45 seconds at 1000 rpm with electron-beam resist 1:3 ZEP-520A/anisole (Zeon) and conductive polymer (Aquasave, Mitsubishi Rayon). Resist was then exposed via electron-beam lithography (CABL9510CC, Crestec). Patterns of 2 μm and 4 μm grids with line widths of 80 nm were fabricated. Conductive polymer was removed by rinsing with deionized water, and then resist was developed for 1 minute in isoamyl acetate. Cr with a thickness

of 7 nm was deposited by electron-beam evaporation (EB3 e-beam evaporator, Edwards). Finally the resist mask is lifted from the coverslip surfaces by sonicating in ice-cold methylene chloride for 10 minutes.

Immunofluorescence staining

Cell cultures were fixed with 4% PFA solution for 10 minutes. PFA solution was washed away with 1x PBS buffer. Fixed cells were blocked with 5% donkey serum (Sigma, Saint. Louis, MO), and permeablised with 0.3% Triton X-100 (EMDminipore, Billerica, MA) for 1 hour. Primary antibody staining was carried out in 4 °C for 48 hours. Mouse antibody to βIII-tubulin (1:500, Sigma, Saint. Louis, MO) and Alexa Fluor 488–conjugated secondary antibodies were used to detect primary antibody (1:250, Jackson Immunoresearch, West Grove, PA). Secondary antibody staining was carried out at room temperature in the dark for 2 hours. DAPI (Life Technologies, Carlsbad, CA) were used to mark nuclei.

Optical microscopy

FRAP, RICM, epifluorescent and bright field images were taken on a motorized inverted microscope (Nikon Eclipse Ti-E/B, Technical Instruments, Burlingame, CA) using a Nikon 100x Apo TIRF 1.49 NA oil immersion objective. The microscope was equipped with a mortorised Epi/TIRF illuminator, a motorized Intensilight mercury lamp, a Nikon Perfect Focus system (Technical Instruments, Burlingame, CA), a motorised stage (ASI MS-2000, Eugene, OR), and an Orca-R2 interline charge-coupled device camera (Hamamatsu, Hamamatsu, Japan). Dichroics were 2 mm thick and mounted in metal cubes to preserve optical flatness: ZT488rdc, ZT561rdc, and ZT640rdc. Three different long-pass emission filters were used: ET500lp, ET575lp, and ET660lp. Bandpass emission filters were installed below the dichroic turret in a motorised filter wheel (Sutter Lambda 10-3, Novato CA): ET525/50m, ET600/50m, ET700/75m, and ET460/50m. RICM was performed using a 50/50 beam splitter with a D546/10 filter. 100 mW 561 nm optically pumped solid-state laser (Coherent Sapphire, Santa Clara CA), and 100 mW 640 nm diode laser (Coherent Cube, Santa Clara CA) were used for TIRF experiments. All FRAP, TIRF, epifluorescent filters and dichroics were purchased from Chroma (Bellows Falls, VT). 20x objective (20x/0.5, DIC M/N2, WD 2.1, Nikon, Technical Instruments, Burlingame, CA) was used to image immunostaining of differentiation studies.

Image analysis

ImageJ/Fuji was used to analyse FRAP data, TIRF data, and immunostaining images. Customized Matlab scripts were then used to analyse the larger data set for corral differentiation. In short, images from immunofluorescent staining were imported into Matlab. Binary images were created for βIII-tubulin channel and DAPI channel. Based on the binary images, fluorescent intensity of each staining cell was recorded, and the numbers of cells stained for βIII-tubulin and DAPI were also recorded. A fluorescent intensity thresholding was set to select cells with positive βIII-tubulin staining. See customized Matlab scripts in Appendix.

Section 3.4: Chapter 3 references

1. Ma DK, Bonaguidi MA, Ming G-l, & Song H (2009) Adult neural stem cells in the mammalian central nervous system. *Cell research* 19(6):672-682.
2. Ming GL & Song H (2011) Adult neurogenesis in the mammalian brain: significant answers and significant questions. *Neuron* 70(4):687-702.
3. Ashton RS*, et al.* (2012) Astrocytes regulate adult hippocampal neurogenesis through ephrin-B signaling. *Nature neuroscience* 15(10):1399-1406.
4. Conway A*, et al.* (2013) Multivalent ligands control stem cell behaviour in vitro and in vivo. *Nature nanotechnology* 8(11):831-838.
5. Shaw A*, et al.* (2014) Spatial control of membrane receptor function using ligand nanocalipers. *Nature methods* 11(8):841-846.
6. Salaita K*, et al.* (2010) Restriction of receptor movement alters cellular response: physical force sensing by EphA2. *Science* 327(5971):1380-1385.
7. Greene AC*, et al.* (2014) Spatial organization of EphA2 at the cell-cell interface modulates trans-endocytosis of ephrinA1. *Biophysical journal* 106(10):2196-2205.
8. Xu Q, Lin WC, Petit RS, & Groves JT (2011) EphA2 receptor activation by monomeric Ephrin-A1 on supported membranes. *Biophysical journal* 101(11):2731-2739.
9. Kaspar D. Mossman GC, Jay T. Groves, Michael L. Dustin. (2005) Altered TCR Signaling from Geometrically Repatterned Immunological Synapses. *Science* 310(5751):1191-1193.
10. Hartman NC, Nye JA, & Groves JT (2009) Cluster size regulates protein sorting in the immunological synapse. *Proceedings of the National Academy of Sciences of the United States of America* 106(31):12729-12734.
11. Manz BN, Jackson BL, Petit RS, Dustin ML, & Groves J (2011) T-cell triggering thresholds are modulated by the number of antigen within individual T-cell

receptor clusters. *Proceedings of the National Academy of Sciences* 108(22):9089-9094.
12. DeMond AL, Mossman KD, Starr T, Dustin ML, & Groves JT (T Cell Receptor Microcluster Transport through Molecular Mazes Reveals Mechanism of Translocation. *Biophysical journal* 94(8):3286-3292.
13. Mossman KD, Campi G, Groves JT, & Dustin ML (2005) Altered TCR Signaling from Geometrically Repatterned Immunological Synapses. *Science* 310(5751):1191-1193.
14. Jackson BL & Groves JT (2004) Scanning Probe Lithography on Fluid Lipid Membranes. *Journal of the American Chemical Society* 126(43):13878-13879.
15. Casaletto JB & McClatchey AI (2012) Spatial regulation of receptor tyrosine kinases in development and cancer. *Nature reviews. Cancer* 12(6):387-400.
16. Hongjun.Song CFS, Fred.H. Gage. (2002) Astroglia induce neurogenesis from adult neural stem cells. *Nature* 417:39-44.
17. Dustin ML & Groves JT (2012) Receptor signaling clusters in the immune synapse. *Annual review of biophysics* 41:543-556.
18. Hilmanen JP (2010) Architecture of Eph receptor clusters. *PNAS* 107(no.24):10860-10865.
19. Himanen JP, Saha N, & Nikolov DB (2007) Cell-cell signaling via Eph receptors and ephrins. *Current opinion in cell biology* 19(5):534-542.
20. Janes PW, Nievergall E, & Lackmann M (2012) Concepts and consequences of Eph receptor clustering. *Seminars in cell & developmental biology* 23(1):43-50.
21. Hilmannen J-P (2001) Crystal structure of an Eph receptor±ephrin complex. *Nature* 414(20/27):933-938.
22. Himanen JP (2012) Ectodomain structures of Eph receptors. *Seminars in cell & developmental biology* 23(1):35-42.
23. Chrencik JE*, et al.* (2006) Structural and biophysical characterization of the EphB4*ephrinB2 protein-protein interaction and receptor specificity. *The Journal of biological chemistry* 281(38):28185-28192.

Chapter 4: Conclusions, Future Directions, and Final Remarks

4.1. Conclusions

Our results have revealed that EphB4 signalling and NSCs functions are sensitive to the spatial and mechanical properties of the apposing membrane on the scale of microns. There results have both spatial and mechanical aspects. Restricting the movement of ephrinB2 ligands indirectly prevents EphB4 receptors from forming large-scale clusters. Physical manipulation of EphB4-ephrinB2 microcluster organisation alters the cellular response to ephrinB2. As a result neuronal differentiation is inhibited.

The mechanical sensitivity of EphB4 receptors is a novel phenomenon that represents a noncanonical receptor force sensing. In our investigations, cells did not respond to integrin receptor associated adhesion machinery because ephrinB2 ligands are the only physical linkages present in the supported membrane. Hence, mechanical forces from diffusion barriers acting on ephrinB2 ligands directly influence EphB4 receptor signalling. Specifically grid barriers that block EphB4 movement in the spatial mutation exert opposing forces on the receptor clusters. Spatial organisation and mechanical forces are likely to be interconnected, resulting in an overall sensitivity of EphB4 signalling pathway in NSC functions to spatio-mechanical aspects of cellular microenvironment in which ephrinB2 ligands are displayed.

Prior studies have shown that EphB4-ephrinB2 signalling that promotes neuronal differentiation is cluster size or ligand concentration dependent. Specifically, larger clusters of receptor-ligand or higher concentration of Fc-ephrinB2 increase the proportion of neuronal differentiation (1, 2). Upon physical restriction of ephrinB2 ligands on supported membrane, EphB4-ephrinB2 clusters are reduced to smaller sizes in micro-corrals. An argument could be made that our results are simply due to a reduction in concentration of ephrinB2 ligands on small gridded size corral membranes, therefore reducing the amount of ephrinB2

available to initiate/active EphB4 signalling. Nevertheless, this argument is not sound. Because the Cr grids serve only as diffusion barriers to restrict the movement of lipid molecules and ephrinB2 ligands, they cannot affect the concentration of ephrinB2 ligands. The number of membrane bound ephrinB2 ligands available to the apposing cell is approximately the same across all different grid sizes. More precisely we have measured the fluorescent intensity of ephrinB2 ligands for all corral membranes before seeding cells for differentiation assays, and we found consistent fluorescent brightness across all conditions. Moreover, we have found no evidence for significant concentration dependence. In particular, we observed no significant differences between ephrinB2 concentration and the proportion of neuronal differentiation when we had tethered lower density of ephrinB2 ligands on supported membrane. Spatial mutation only disrupts the local concentration of ephrinB2 in each individual clusters. Therefore, our results demonstrate that neuronal differentiation by EphB4-ephrinB2 signalling is modulated by the spatial and mechanical organisation of receptor-ligand at the membrane-cell interface.

4.2. Future Directions

Explore the molecular mechanism of EphB4-ephrinB2 signalling under spatial mutation

We have already demonstrated an effect from spatial mutation on neural stem cell differentiation. Specifically, neuronal differentiation is regulated by the spatial and mechanical manipulation of EphB4 receptor signalling. It will be critical to determine what is changing at the molecular and cellular levels when physical constraints are applied to NSC surface receptors. Future work will be aimed at understanding whether any of the EphB4 signalling components are sensitive to the spatio-mechano-disruption created by physical constraints, since this alteration may directly regulate NSC functions.

To attain this aim, we will first develop an assay to detect EphB signalling molecules recruitment and activation of downstream effectors. We will then employ spatial mutation to explore cellular changes of these signalling components. We will combine biochemical and advanced imaging techniques together for this sub-aim. We have selected several target molecules to test based on their activities in EphB signaling in early studies, for example, Src and PI-3

kinases have been shown to be regulated upon activation of EphB4-ephrinB2 signalling (3-5). We will test out these identified signalling components first. We hypothesise that downstream recruitment and signal effectors should be activated in close contact to the EphB4-ephrinB2 signalling vicinity, which would be present at Eph-ephrin clusters. First, we will look for the presence of these molecules in neural stem cells using a Western blot analysis and immunofluorescent staining. Second, we will apply high resolution TIRF microscopy to determine if these molecules are co-localised with the Eph-ephrin cluster. We also want to confirm these signalling molecules are activated upon Eph-ephrin clustering, for example by analysing their phosphorylation levels.

Next, we will employ spatial mutation to study the response of these signalling molecules to mechanical perturbations and spatial reorganisation of EphB4-ephrinB2 signalling. Specifically, we will control the size of receptor-ligand clusters by restricting the lateral mobility of lipids and membrane proteins using fabricated micro-corrals. Using TIRF, we will measure changes in Eph-ephrin cluster size and dynamics, cytoskeletal protein morphology, and the behaviour of signalling components. We hypothesise a correlation between physical restrictions of receptor-ligand coupling and the cellular response of signalling molecules: activation/recruitment of signalling molecules will be regulated by physical reorganisation of EphB4 receptor. If this hypothesis is verified, we will further investigate the molecular mechanism of stem cell differentiation in the Eph-ephrin dependent pathway. We will repeat stem cell differentiation studies on ephrin-bilayers, this time inhibiting these mechanosensitive molecules through drugs or mutations. If stem cell differentiation is affected, then these molecules are likely directly involved in EphB4 downstream signalling. Spatial mutation technique can be therefore used as a novel means to probe "gain and loss of function" of mechanosensitive signalling molecules.

4.3. Final Remarks

Supported lipid bilayers serve as a versatile platform for recapitulating the physical microenvironment of cell-cell contact dependent signalling in NSCs. It is also a robust system for investigating the effects of spatial reorganisation in EphB4 signalling. Our results provide a critical understanding of how EphB4-ephrinB2 signalling in NSCs responds to receptor-ligand physical constraints and protein spatial reorganisation. Future studies exploring the molecular mechanism of EphB4-ephrinB2 signalling under spatial mutation will be critical. In particular, if we discover that the precise spatial-mechanical control of signal clusters at the intercellular junction can regulate neural stem cell lineage commitment, then we

will have discovered a novel mechanism for cellular differentiation control. Eventually, we hope to integrate and apply this knowledge into future tissue engineering and regenerative medicine in order to control stem cell behaviour.

4.4. Chapter 4 references

1. Ashton RS*, et al.* (2012) Astrocytes regulate adult hippocampal neurogenesis through ephrin-B signaling. *Nature neuroscience* 15(10):1399-1406.
2. Conway A*, et al.* (2013) Multivalent ligands control stem cell behaviour in vitro and in vivo. *Nature nanotechnology* 8(11):831-838.
3. Steinle JJ*, et al.* (2002) Eph B4 receptor signaling mediates endothelial cell migration and proliferation via the phosphatidylinositol 3-kinase pathway. *The Journal of biological chemistry* 277(46):43830-43835.
4. Peltier J, O'Neill A, & Schaffer DV (2007) PI3K/Akt and CREB regulate adult neural hippocampal progenitor proliferation and differentiation. *Developmental neurobiology* 67(10):1348-1361.
5. Genander M*, et al.* (2009) Dissociation of EphB2 signaling pathways mediating progenitor cell proliferation and tumor suppression. *Cell* 139(4):679-692.

Appendix

We used the following function in Matlab for differentiation analysis: this function is used to automate handcounting by looping through a series of folders. For each, raw data are binarised and masked, objects are removed from the edges and if larger than a cutoff number of pixels (here, we set the cutoff to 200 pixels).

```
Folders = dir([DataDir FolderStr]);
for ii = 1:size(Folders,1)
  close all
  Files = dir([DataDir Folders(ii).name '/' NumStr]);
ff=1;
  while ff<=size(Files,1)
    try
      Data = dir([DataDir Folders(ii).name '/' Files(ff).name '/' FileStr1]);
      image = imread([DataDir Folders(ii).name '/' Files(ff).name '/' Data.name]);
[LEVEL, EM] = graythresh(image);
      imagebinary = im2bw(image, graythresh(image));
imagebinarynoholes = imfill(imagebinary,'holes');
imagebinarynoholesbig = bwareaopen(imagebinarynoholes,400);
imagebinarynoholesbigborder = imagebinarynoholesbig;

[eachcell, count] = bwlabel(imagebinarynoholesbigborder);
      eachcellinfo=regionprops(eachcell,image,'all');
```

```
                Data2 = dir([DataDir Folders(ii).name '/' Files(ff).name '/'
FileStr2]);
                image2 = imread([DataDir Folders(ii).name '/' Files(ff).name
'/' Data2.name]);

                warning('off','images:initSize:adjustingMag');

            [LEVEL, EM] = graythresh(image2);
                imagebinary2 = im2bw(image2, graythresh(image2));
            imagebinarynoholes2 = imfill(imagebinary2,'holes');
            imagebinarynoholesbig2 = bwareaopen(imagebinarynoholes2,200);
                imagebinarynoholesbigborder2 = imagebinarynoholesbig2;

                [eachcell2, count2] = bwlabel(imagebinarynoholesbigborder2);
                eachcellinfo2=regionprops(eachcell2,image2,'all');

                Data3 = dir([DataDir Folders(ii).name '/' Files(ff).name '/'
FileStr3]);
                image3 = imread([DataDir Folders(ii).name '/' Files(ff).name
'/' Data3.name]);

                warning('off','images:initSize:adjustingMag');

            [LEVEL, EM] = graythresh(image3);
                imagebinary3 = im2bw(image3, graythresh(image3));
```

```
imagebinarynoholes3 = imfill(imagebinary3,'holes');
imagebinarynoholesbig3 = bwareaopen(imagebinarynoholes3,200);
imagebinarynoholesbigborder3 = imagebinarynoholesbig3;
[eachcell3, count3] = bwlabel(imagebinarynoholesbigborder3);
eachcellinfo3=regionprops(eachcell3,image3,'all');


screen_size = get(0,'ScreenSize');


h1 = figure(1);
set(gcf, 'name', [Folders(ii).name '/' Files(ff).name]);
imshow(image2,[0
max(max(image2*0.5))],'InitialMagnification',25)
set(gcf,'Position',[650 900 screen_size(3)*0.30
screen_size(4)*0.35]);
text(25,60,'Nuclei','fontsize',20,'color',[1 1 1])
hold off
h2 = figure(2);
set(gcf, 'name', [Folders(ii).name '/' Files(ff).name]);
imshow(image3,[0
max(max(image2))],'InitialMagnification',25)
set(gca,'Visible','off');
set(gcf,'Position',[650 0 screen_size(3)*0.30 screen_size(4)*0.35]);
set(gca,'NextPlot','add');
set(gcf,'InvertHardCopy','off');
set(gcf,'PaperPositionMode','auto');
```

```
                text(25,60,'GFAP','fontsize',20,'color',[1 1 1])


                h3 = figure(3);

                set(gcf, 'name', [Folders(ii).name '/' Files(ff).name]);

imshow(imagebinarynoholesbigborder,'InitialMagnification',25)

                set(gca,'Visible','off');

                set(gcf,'Position',[1050 900 screen_size(3)*0.30
screen_size(4)*0.35]);

                set(gca,'NextPlot','add');

                set(gcf,'InvertHardCopy','off');

                set(gcf,'PaperPositionMode','auto');

                text(25,60,'Tubulin Binary','fontsize',20,'color',[1 1 1])


                h4 = figure(4);

                set(gcf, 'name', [Folders(ii).name '/' Files(ff).name]);

                imshow(image,[0
max(max(image*0.25))],'InitialMagnification',25)

                set(gca,'Visible','off');

            set(gcf,'Position',[1050 0 screen_size(3)*0.30 screen_size(4)*0.35]);

                set(gca,'NextPlot','add');

                set(gcf,'InvertHardCopy','off');

                set(gcf,'PaperPositionMode','auto');

                text(25,60,'Tubulin Raw','fontsize',20,'color',[1 1 1])
```

```
query=input('action (1=continue,2=skip,3=redo): ');
while length(query)==0
   query=input('action (1=continue,2=skip,3=redo): ');
end

if query == 2
   ff=ff+1;
   continue;
end

if query == 3
   continue;
end



j=1;
k=1;
dontkeep=[];

for i = 1:length(eachcellinfo)

rectangle('Position',eachcellinfo(i).BoundingBox,'EdgeColor','g','LineWidth',2)
```

```
                response=input('cells in box (press enter if 1): ');

                if response == 0
rectangle('Position',eachcellinfo(i).BoundingBox,'EdgeColor','r','LineWidth',2);
                    dontkeep(j)=i;
                    j=j+1;
                else
                    text(eachcellinfo(i).BoundingBox(1)-
20,eachcellinfo(i).BoundingBox(2)-20,num2str(k),'Color', 'w')
                    k=k+1;
                    if isempty(response)
                        eachcellinfo(i).Multiplicity=1;
                    else
                        eachcellinfo(i).Multiplicity=response;
                    end
rectangle('Position',eachcellinfo(i).BoundingBox,'EdgeColor','b','LineWidth',2)
                end


            end

            hold off
```

```
                eachcellinfo(dontkeep)=[];


                output=eachcellinfo;


            mkdir([DataDir Folders(ii).name '/' Files(ff).name '/Results']);

                Results = [output.MeanIntensity; output.MaxIntensity;
output.MinIntensity];

                save([DataDir Folders(ii).name '/' Files(ff).name
'/Results/Counts_Tublin'],'Results');


            textstr1 = strfind(FileStr1,'*');

            set(h3,'Position',[1050 900 screen_size(3)*0.30
screen_size(4)*0.35]);

                set(h3,'NextPlot','add');

                set(h3,'InvertHardCopy','off');

                set(h3,'PaperPositionMode','auto');

                saveas(h3,[DataDir Folders(ii).name '/' Files(ff).name
'/Results/BinaryImage_' num2str(FileStr1(textstr1(1,1)+1:textstr1(1,2)-1))
'.tif'],'tif')

                hold on


            set(h4,'Position',[1050 0 screen_size(3)*0.30 screen_size(4)*0.35]);

                set(h4,'NextPlot','add');

                set(h4,'InvertHardCopy','off');

                set(h4,'PaperPositionMode','auto');

                saveas(h4,[DataDir Folders(ii).name '/' Files(ff).name
```

```
'/Results/BoxedImage_' num2str(FileStr1(textstr1(1,1)+1:textstr1(1,2)-1))
'.tif'],'tif')
                    hold on


                    figure(5);
                    set(gcf, 'name', [Folders(ii).name '/' Files(ff).name]);

imshow(imagebinarynoholesbigborder2,'InitialMagnification',25)
                    set(gcf,'Position',[650 900 screen_size(3)*0.30
screen_size(4)*0.35]);
                    text(25,60,'Nuclei','fontsize',20,'color',[1 1 1])


                    j=1;
                    k=1;
                    dontkeep=[];

                    for i = 1:length(eachcellinfo2)


rectangle('Position',eachcellinfo2(i).BoundingBox,'EdgeColor','g','LineWidth',2)


                      response=input('cells in box (press enter if 1): ');


                      if response == 0

rectangle('Position',eachcellinfo2(i).BoundingBox,'EdgeColor','r','LineWidth',2);
```

```
                dontkeep(j)=i;
                j=j+1;
            else
                text(eachcellinfo2(i).BoundingBox(1)-
20,eachcellinfo2(i).BoundingBox(2)-20,num2str(k),'Color', 'w')
                k=k+1;
                if isempty(response)
                    eachcellinfo2(i).Multiplicity=1;
                else
                    eachcellinfo2(i).Multiplicity=response;
                end

rectangle('Position',eachcellinfo2(i).BoundingBox,'EdgeColor','b','LineWidth',2)
            end
        end

        hold off

        temp = [eachcellinfo2.Multiplicity];
        NucleiCount = sum(temp);
        save([DataDir Folders(ii).name '/' Files(ff).name
'/Results/TotalCells'],'NucleiCount');

        h6 = figure(6);
        set(gcf, 'name', [Folders(ii).name '/' Files(ff).name]);
```

```
imshow(imagebinarynoholesbigborder3,'InitialMagnification',25)
                screen_size(4)*0.35]);
                    set(gcf,'Position',[650 0 screen_size(3)*0.30
screen_size(4)*0.35]);
                    text(25,60,'GFAP','fontsize',20,'color',[1 1 1])

                    j=1;
                    k=1;
                    dontkeep=[];

                    for i = 1:length(eachcellinfo3)

rectangle('Position',eachcellinfo3(i).BoundingBox,'EdgeColor','g','LineWidth',2)

                      response=input('cells in box (press enter if 1): ');

                      if response == 0

rectangle('Position',eachcellinfo3(i).BoundingBox,'EdgeColor','r','LineWidth',2);
                        dontkeep(j)=i;
                        j=j+1;
                      else
                        text(eachcellinfo3(i).BoundingBox(1)-
20,eachcellinfo3(i).BoundingBox(2)-20,num2str(k),'Color', 'w')
```

```
                    k=k+1;
                    if isempty(response)
                       eachcellinfo3(i).Multiplicity=1;
                    else
                       eachcellinfo3(i).Multiplicity=response;
                    end

rectangle('Position',eachcellinfo3(i).BoundingBox,'EdgeColor','b','LineWidth',2)
                  end
                end

                hold off

                output = eachcellinfo3;
            Results = [output.MeanIntensity; output.MaxIntensity;
output.MinIntensity];
                save([DataDir Folders(ii).name '/' Files(ff).name
'/Results/Counts_GFAP'],'Results');

                textstr1 = strfind(FileStr3,'*');
            set(h6,'Position',[650 200 screen_size(3)*0.20 screen_size(4)*0.35]);
                set(h6,'NextPlot','add');
                set(h6,'InvertHardCopy','off');
                set(h6,'PaperPositionMode','auto');
                saveas(h6,[DataDir Folders(ii).name '/' Files(ff).name
'/Results/BoxedImage_' num2str(FileStr3(textstr1(1,1)+1:textstr1(1,2)-1))
```

```
'.tif'],'tif')
                ff=ff+1;
                catch
                   continue
                end
              end
            end

            close all
```